Projecting global drought risk under various SSP-RCP scenarios

Zhiling Zhou[1], Liping Zhang[1], Jie Chen[1], Dunxian She[1], Gangsheng Wang[1], Qin Zhang[1], Jun Xia[1], and Yanjun Zhang[1]

[1]Wuhan University

November 23, 2022

Abstract

Drought risk assessment can identify high-risk areas and bridge the gap between impacts and adaptation. However, very few dynamic drought risk assessments and projections have been performed worldwide at high spatial resolution (e.g., 0.5{degree sign} × 0.5{degree sign}) under different greenhouse gas emission scenarios. Here, future global drought risk is projected combing three components (i.e., hazard, exposure, and vulnerability) during 2021-2100 under combined scenarios of Representative Concentration Pathways (RCPs) and Shared Socioeconomic Pathways (SSPs): SSP1-2.6, SSP2-4.5, SSP3-7.0, and SSP5-8.5. This study first investigates dynamic drought risks and exposed population and GDP across the six continents (Antarctica is not examined due to data availability). The results show that high-risk regions mainly concentrate in southeastern China, India, Western Europe, eastern United States, and western and eastern Africa. Drought risk will further strengthen in the future under four scenarios, with the highest under SSP5-8.5 and the lowest under SSP3-7.0. Populations exposed to high drought risk for Asia and Africa are much more than other continents. Among four SSP-RCPs, populations exposed to high risk are the largest under SSP3-7.0 for Africa, Asia, and South America, while under SSP5-8.5 for Australia, Europe, and North America. GDP exposed to high drought risk is the largest for Asia among the six continents and the largest under SSP5-8.5 among the SSP-RCPs. The most significant increases in population and GDP under high drought risk both occur in Africa. This study provides a scientific basis for effective adaptation measures to enhance drought resilience in potential high-risk areas.

Projecting global drought risk under various SSP-RCP scenarios

Zhiling Zhou[1], Liping Zhang[1,2]*, Jie Chen[1], Dunxian She[1,2], Gangsheng Wang[1,2], Qin Zhang[1], Jun Xia[1,2], Yanjun Zhang[1,2]

[1]State Key Laboratory of Water Resources and Hydropower Engineering Science, Wuhan University, Wuhan 430072, P. R. China.

[2]Institute for Water-Carbon Cycles and Carbon Neutrality, Wuhan University, Wuhan 430072, P. R. China.

Corresponding author: Liping Zhang (zhanglp@whu.edu.cn)

Key Points:

(1) We present dynamic future global drought risk maps under four SSP-RCP scenarios.

(2) Drought risk will increase worldwide in the future, especially under SSP5-8.5.

(3) Among the six continents, the population and GDP under high drought risk are the most in Asia and the fastest growing in Africa.

Abstract

Drought risk assessment can identify high-risk areas and bridge the gap between impacts and adaptation. However, very few dynamic drought risk assessments and projections have been performed worldwide at high spatial resolution (e.g., 0.5° × 0.5°) under different greenhouse gas emission scenarios. Here, future global drought risk is projected combing three components (i.e., hazard, exposure, and vulnerability) during 2021–2100 under combined scenarios of Representative Concentration Pathways (RCPs) and Shared Socioeconomic Pathways (SSPs): SSP1-2.6, SSP2-4.5, SSP3-7.0, and SSP5-8.5. This study first investigates dynamic drought risks and exposed population and GDP across the six continents (Antarctica is not examined due to data availability). The results show that high-risk regions mainly concentrate in southeastern China, India, Western Europe, eastern United States, and western and eastern Africa. Drought risk will further strengthen in the future under four scenarios, with the highest under SSP5-8.5 and the lowest under SSP3-7.0. Populations exposed to high drought risk for Asia and Africa are much more than other continents. Among four SSP-RCPs, populations exposed to high risk are the largest under SSP3-7.0 for Africa, Asia, and South America, while under SSP5-8.5 for Australia, Europe, and North America. GDP exposed to high drought risk is the largest for Asia among the six continents and the largest under SSP5-8.5 among the SSP-RCPs. The most significant increases in population and GDP under high drought risk both occur in Africa. This study provides a scientific basis for effective adaptation measures to enhance drought resilience in potential high-risk areas.

Plain Language Summary

Drought increasingly affects society, economy, and ecosystems as a frequent natural disaster. Drought risk assessment can help understand the extent of drought threat to the human system. However, there are very few global drought risk assessments and projections at high spatial resolution under various climate change scenarios. Therefore, we projected 0.5° × 0.5° future drought risk during 2021-2100 under four scenarios and investigated exposed population and GDP across the six continents (Antarctica is not examined due to data availability). We find that high-risk regions mainly concentrate in southeastern China, India, Western Europe, eastern United States, and western and eastern Africa. Global drought risk will increase in the future. Populations exposed to high drought risk for Asia and Africa are much more than other continents. GDP exposed to

high drought risk is the largest for Asia among the six continents. The most significant increases in population and GDP under high drought risk both occur in Africa. Our findings help policymakers develop adaptive disaster prevention measures.

1. Introduction

Drought is one of the major severe natural disasters which leads to enormous damage and costs (Lesk et al., 2016; Spinoni et al., 2014). It affects millions of people each year and adversely impacts society, economy, and environment worldwide (Marengo et al., 2017; Spinoni et al., 2018; Vicente-Serrano et al., 2020). The United Nations Office for Disaster Risk Reduction (UNDRR) stated that people affected by drought accounted for 35 percent of all natural disasters in the past two decades (ISFD Reduction, 2004). Among the top ten worldwide disasters in the past 50 years (1970–2019), drought was the deadliest, causing 650,000 deaths and far more economic losses than other meteorological disasters (WMO, 2021). It is illustrated that drought has become a worldwide problem and attached adverse effects to the globe.

In the context of global warming, the frequency and severity of droughts have increased at the global and regional scales (Naumann et al., 2018; Takeshima et al., 2020; Touma et al., 2015; Ukkola et al., 2020). Moreover, land areas affected by increasing drought frequency and severity will expand under global warming with high confidence as per the recently published Sixth Assessment Report of the IPCC Working Group I (IPCC, 2021). Society and the economy will continuously grow simultaneously, leading to more losses under droughts in the future (Su et al., 2018). Thus predicting future drought risk is crucial for disaster prevention and reduction decision-making.

Drought risk refers to the possibility of dramatic detrimental changes due to hazardous drought events interacting with vulnerable social conditions and ultimately resulting in widespread adverse impacts in a community or system (IPCC, 2012). Different from drought conditions, drought risk is determined not only by the intensity of drought events but also by the exposure of the social-economic system and its susceptible characteristics. Thus, drought risk is generally quantified by three primary components: hazard, exposure, and vulnerability (Chou et al., 2019; Le et al., 2021; Prabnakorn et al., 2019). Hazard is the physical natural drought-related characteristics. Exposure refers to the presence of population and assets in places that can be affected, and vulnerability is the system's feature contributing to a tendency or predisposition to adversely impacts

(Carrao et al., 2016; IPCC, 2012; Meza et al., 2020). Drought risk has been assessed by combing hazard, exposure, and vulnerability for various regions (Guo et al., 2021; M. A. A. Hoque et al., 2021; Sahana et al., 2021). In addition, pertaining to various specific sectors, such as water resource, agriculture, and ecological goals, a variety of attempts have been taken with different indicators of hazard, exposure, and vulnerability to assess drought risk (Dai et al., 2020; X. Liu et al., 2021; Meza et al., 2020). One of the critical points in drought risk assessment is the selection of indicators. Indices can be specific in small regions (Khoshnazar et al., 2021; Kim et al., 2020). However, when focusing on giant areas, it is a challenge to concurrently account for the comprehensiveness, accuracy, and accessibility of the indicators. Population, economy, and land-use patterns were generally considered (Ahmadalipour et al., 2019; Y. J. Liu & Chen, 2021). Remote sensing data and GIS tools were widely applied (Palchaudhuri & Biswas, 2016; Sun et al., 2014). Administrative areas were generally employed as the spatial unit during drought risk assessment because socioeconomic data were customarily collected by administrative regions (Ahmadalipour et al., 2019; Kim et al., 2020), leading to a relatively coarse spatial resolution. In recent decades, the prosperous development of climate models (Lehner et al., 2017; Thilakarathne & Sridhar, 2017; Y. Y. Yin et al., 2021) has provided spatially accurate (e.g., below $1° \times 1°$ grid) projected climate data, making it possible to project future drought risk with a relatively high spatial resolution. Risk predictions can contribute to distinguishing the future high-risk regions and identifying the risk change for specific regions.

Nevertheless, there are few consistent assessments and future projections across the globe considering both climate change and socioeconomic developments. In addition, there is a lack of predictions of populations and GDP exposed to high drought risk at continental scale. In this study, we assessed global drought risk in the historical period (1991–2014) and future period (2021–2100) under four climate scenarios using global climate models (GCMs) in the Coupled Model Intercomparison Project Phase 6 (CMIP6). The four scenarios were newly proposed in CMIP6 as a combination of Representative Concentration Pathways (RCPs) and Shared Socioeconomic Pathways(SSPs): SSP1-2.6, SSP2-4.5, SSP3-7.0, and SSP5-8.5 (O'Neill et al., 2016). We simultaneously considered future drought changes, population and economic development, and land-use change under various SSP-RCP scenarios. In addition, we Figured the exposed population and GDP for six continents (Antarctica is not examined due to data availability). The aims of this study are to (1) quantify the global drought risks at a $0.5° \times 0.5°$ resolution under four

SSP-RCP scenarios based on the up-to-date CMIP6 GCMs and dynamic projected socioeconomic data; and (2) project future drought risks and associated affected population and economy under high drought risk at continental scale.

2. Materials and methods

2.1. Data

GCMs are widely used for the projection of future climate (Cook et al., 2020; Su et al., 2021; Zheng et al., 2018). Simulations including precipitation and surface maximum air temperature were obtained from the GCM outputs in CMIP6. Three GCMs were selected in this study based on their ability in the simulations of extreme precipitation (Ayugi et al., 2021; Dong & Dong, 2021; Sian et al., 2021; Tang et al., 2021). The details of the three GCMs are shown in Table 1. The projection experiment in CMIP6 contains a new set of emissions and land-use scenarios that combines five SSPs and four RCPs (Riahi et al., 2017; van Vuuren et al., 2014). In this work, four combined scenarios in Tier-1 (SSP1-2.6, SSP2-4.5, SSP3-7.0, and SSP5-8.5) were selected to assess the drought hazard in the future period. A bilinear interpolation scheme was applied to interpolate the three GCMs to a common 0.5° × 0.5° grid. Bias correction was conducted with the Quantile Mapping method using observation data from Climate Prediction Center (CPC) in 1979–2014 as baselines.

Global 1 km population data during 2000–2014 were from WorldPop (Lloyd et al., 2019). Annual population data in 1991–1999 were linearly interpolated using 1 km population data in 1990, 1995, and 2000 from Global Rural-Urban Mapping Project, Version 1 (Balk et al., 2006; Center for International Earth Science Information Network - CIESIN - Columbia University et al., 2011). Annual GDP data with a spatial resolution of 5 arc-min during 1991–2014 (Kummu et al., 2018) were used. The historical population and GDP data were re-gridded to 0.5° spatial resolution. Global 0.5° × 0.5° population and GDP projections under the four SSP scenarios (Huang et al., 2019; Jiang, Wang, et al., 2018; Jiang, Zhao, et al., 2018; Jing et al., 2020; Mondal et al., 2021) were employed for exposure and vulnerability calculations. Annual historical land cover data were gained from European Space Agency (ESA) with a 300 m spatial resolution. Global 0.1° × 0.1° land cover projections from 2020 to 2100 under different RCP scenarios (Fan et al., 2013, 2015; Fan, Bai, et al., 2020; Fan, Li, et al., 2020; Yue et al., 2005, 2006, 2007) were utilized. Resample and zonal statistics tools in ArcGIS were used to uniform the resolution to 0.5°. The 5 min × 5 min road density data (Meijer et al., 2018) were used and resampled to 0.5° × 0.5°. The linear density statistics tool in ArcGIS was processed to get the 0.5° × 0.5° channel density using the river network data (Yan et al., 2019). Based on these data, the hazard, exposure, vulnerability, and risk of drought were quantified for the historical and future periods under four SSP-RCP scenarios.

Table 1.
Information of the global climate models.

Model	Institution	Resolution (Lon×Lat)	Calendar
EC-Earth3	EC-Earth-Consortium, Europe	0.7°×0.7°	gregorian
NorESM2-LM	Norwegian Climate Centre, Norway	2.5°×1.9°	365day
NorESM2-MM	Norwegian Climate Centre, Norway	1.25°×0.94°	365day

2.2. Quantification of drought risk

According to the risk definition proposed by the Intergovernmental Panel on Climate Change (IPCC, 2014), drought risk is assessed through indicators of three determinants: hazard, exposure, and vulnerability. The risk was calculated using the formulation implemented by the United Nations International Strategy for Disaster Reduction (Pearson & Pelling, 2015) and IPCC (IPCC, 2012) in this study, and it has been applied in many earlier risk assessments (Ahmadalipour et al., 2019; Carrao et al., 2016; Peduzzi et al., 2009). It is defined as:

$$\mathrm{Risk} = \mathrm{Hazard}^{W_H} \times \mathrm{Exposure}^{W_E} \times \mathrm{Vulnerability}^{W_V} \qquad (1)$$

where W_H, W_E, W_V are the weights for hazard, exposure, and vulnerability (Table 2).

2.2.1 Drought hazard (DH)

Hazard refers to the physical natural events that may cause disasters to human society. Standardized precipitation index (SPI; Guttman, 1999; McKee et al., 1993) was used to analyze the drought hazard in the baseline and projected periods. The SPI can quantify the lack of precipitation over multiple time scales based on the normalized probability distribution of cumulative precipitation series. It has been widely applied in drought studies because of its universality and simplicity of calculation (Dabanli et al., 2017; Dashtpagerdi et al., 2015; Kim et al., 2020). In order to identify the short-duration drought, the precipitation was cumulated every ten days, and each ten-days was fitted separately (Khoshnazar et al., 2021). Then a 3-ten-days moving average was applied to calculate the SPI.

Three drought characteristics were calculated from the SPI: drought severity (DS), drought frequency (DF), and drought duration (DD). Based on the run theory (Figure 1), a drought starts when the SPI value falls below the threshold and ends when the value rises above the threshold again. The threshold is -1 in this study according to McKee's classification (McKee et al., 1993). Drought frequency is the number of drought events in a year. Drought duration is the number of time units (ten days in this study) between the start and the end of droughts. Drought severity is the integral of the area confined between the horizontal line below -1 and the start-end points of a drought event. If there were more than one drought in a year, we calculated the average value of DD and DS.

In addition to the three drought characteristics, continuous dry days (CDD) and the max temperature (TM) were also used to calculate DH. Continuous dry days are often closely associated with drought, and high temperature leads to more evaporation and contributes to drought (Cai et al., 2009). The indicator values of the three models were averaged. Thus drought hazard was calculated as:

$$\mathrm{DH} = \mathrm{DS}^{\mathrm{W_{DS}}} \times \mathrm{DF}^{\mathrm{W_{DF}}} \times \mathrm{DD}^{\mathrm{W_{DD}}} \times \mathrm{CDD}^{\mathrm{W_{CDD}}} \times \mathrm{TM}^{\mathrm{W_{TM}}} \quad (2)$$

where DS, DF, DD, CDD, and TM represent the drought severity, drought frequency, drought duration, continuous dry days, and the max temperature, respectively, and $\mathrm{W_{DS}}$, $\mathrm{W_{DF}}$, $\mathrm{W_{DD}}$, $\mathrm{W_{CDD}}$, and $\mathrm{W_{TM}}$ are weights for DS, DF, DD, CDD, and TM, respectively.

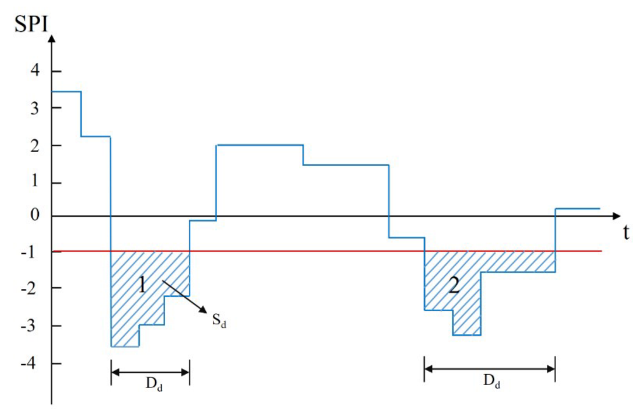

Figure 1. Schema of the run theory where D_d is the drought duration and S_d is the drought severity.

2.2.2 Drought exposure (DE)

Exposure is defined as the presence of people and economic assets in places and settings that can be adversely affected (IPCC, 2012). In this study, population and GDP were used to describe the drought exposure considering population and economy are the most directly affected by drought disasters in socioeconomic systems (Y. J. Liu & Chen, 2021). Here the GDP refers to the total economic output for each grid. Drought exposure was calculated as:

$$\mathrm{DE} = \mathrm{PEO}^{\mathrm{W_{PEO}}} \times \mathrm{GDP}^{\mathrm{W_{GDP}}} \quad (3)$$

where PEO and GDP represent the population (million persons) and total economic output (hundred million US dollars in 2010 price) for each grid. $\mathrm{W_{PEO}}$ and $\mathrm{W_{GDP}}$ are the weights for PEO and GDP, respectively.

2.2.3 Drought vulnerability (DV)

IPCC defined vulnerability as the property of the system's propensity to be adversely affected (IPCC, 2012). The hybrid index-based approach was the most common method used in vulnerability assessment. Despite its limitation for policy effects, composite indicators can identify standard evaluation guidelines for impact reduction on the regional to global scale (Meza et al., 2020). The United Nations International Strategy for Disaster Reduction (UNISDR) proposed a drought vulnerability framework to reflect the state of the social, economic, and infrastructural factors of a region (Reduction, 2004). Disaster prevention and mitigation capabilities are also incorporated into vulnerability considerations. These factors are mainly reflected and quantized by generic indicators related to a specific exposed element (Carrao et al., 2016). In consideration of both the representativeness of indicators and the availability of data, we chose four indicators: (1) ratio of the cropland and built-up land in a grid (LU), reflecting the agricultural and infrastructural factors of vulnerability, (2) road density (RD), reflecting infrastructural factors and transport capacity in disaster relief, (3) channel density (CD), reflecting the local water resource condition, and (4) the GDP per capita (GDPP), reflecting the local financial level and disaster bearing capacity. Drought vulnerability was calculated as:

$$\mathrm{DV} = \mathrm{LU}^{\mathrm{W_{LU}}} \times \mathrm{RD}^{\mathrm{W_{RD}}} \times \mathrm{CD}^{\mathrm{W_{CD}}} \times \mathrm{GDPP}^{\mathrm{W_{GDPP}}} \quad (4)$$

where $\mathrm{W_{LU}}$, $\mathrm{W_{RD}}$, $\mathrm{W_{CD}}$, and $\mathrm{W_{GDPP}}$ are the weights for LU, RD, CD, and GDPP.

2.3. Normalization of indicators

After aggregating raw values of each indicator, a linear scale normalization (OECD, 2008) was performed to standardize all index values to an identical range of 0 to 1. The normalization is performed by considering the maximum and minimum values of each indicator among all grids. For indicators with positive (+) and negative (-) correlations to drought risk (see Table 2), the normalization was calculated as:

$$\begin{cases} Z_i = \frac{X_i - X_{\min}}{X_{\max} - X_{\min}} \times 10 & \text{positive correlation} \\ Z_i = \left(1 - \frac{X_i - X_{\min}}{X_{\max} - X_{\min}}\right) \times 10 & \text{negative correlation} \end{cases} \tag{5}$$

where Z_i and X_i represent the normalized and raw indicator value for grid *i*, respectively, $X_{\max}$ and $X_{\min}$ represent the maximum and minimum values across all grids.

Finally, hazard, exposure, or vulnerability was calculated by multiplying the indicators with exponential weights:

$$Y = \prod Z_i^{W_i} \tag{6}$$

where Y is the hazard/exposure/vulnerability, and W_i is the weight for each indicator.

2.4. Weighting indicators using the Analytic Hierarchy Process

Analytical Hierarchy Process (AHP) is a flexible method to analyze complex multi-criteria decisions (Saaty & Vargas, 2001), and has been widely utilized to determine the weight of indicators in comprehensive evaluation (M. A. Hoque et al., 2020; Mokarram et al., 2021; Palchaudhuri & Biswas, 2016; Sahana et al., 2021). The weight is determined by the relative importance among the criteria through a pairwise comparison. The consistency index (CI) and the consistency ratio (CR) were used to examine the logical consistency of the weights:

$$\mathrm{CI} = (\lambda_{\max} - n)/(n - 1) \tag{7}$$

$$\mathrm{CR} = \mathrm{CI}/\mathrm{RI} \tag{8}$$

where *n* is the number of objects to compare, $\lambda_{\max}$ is the largest eigenvalue of the pairwise comparison matrix, and RI is the randomly generated average consistency index.

More details of the AHP procedure can be found in Saaty (1987). Generally, the closer a CR is to zero, the more consistent the weights are. In this study, CR values <0.1 were permitted. The weights were shown in Table 2.

Table 2.
Drought risk assessment model.

		Weight 1*	Indicators (correlation)	Weight 2*	Weight 1×weight 2*
Drought risk	Hazard	0.4	DS (+)	0.219	0.088
			DF (+)	0.258	0.103
			DD (+)	0.219	0.088
			CDD (+)	0.110	0.044
			TM (+)	0.194	0.078
	Exposure	0.25	POP (+)	0.5	0.125
			GDP (+)	0.5	0.125
	Vulnerability	0.35	LU (+)	0.192	0.067
			RD (-)	0.144	0.050
			CD (-)	0.349	0.122
			GDPP (-)	0.315	0.110

Note. Weight 1 is the weight of hazard, exposure, and vulnerability (equation (1)); weight 2 is the weight of each indicator in hazard, exposure, or vulnerability (equation (2), (3), (4)).

3. Results

In this section, global drought hazard, exposure, vulnerability, and risk were calculated annually in the baseline period (1991–2014) and the future period (2021–2100) under four scenarios. The global maps of the four outcomes demonstrate the average value of the historical period (1991–2014) and three future periods (near-term, 2021–2040; mid-term, 2041–2060; long-term, 2081–2100).

3.1. Spatiotemporal variation in drought hazard

Figure 2 shows the global distribution of drought hazard in the baseline period and the three projected periods under SSP2-4.5 (maps under the other three scenarios are provided in Figures S1–S3 in supplementary materials). The value of drought hazard (i.e., the product of the five normalized indicators) varies from 0 to 3.6. Generally, the spatial distribution is relatively constant, and the high levels of hazard (dark orange to red color scheme) are spatially concentrated. High drought hazard occurs in central Brazil, southwestern North America, northern and southern Africa, southern Europe, northern Middle East, and Australia. When examining the temporal change of drought hazard, it appears to be more severe in the projected periods than the baseline periods. For the future period, the average global drought hazard is projected to keep increasing (Figure 3b). A transparent increasing trend can be found in high drought hazard areas (dark orange to red color scheme) while there is little change in moderate drought hazard areas (yellow color scheme) (Figure 2). The most significant change in drought hazard over time is located in central Brazil, followed by southern Africa. Hazard in high-hazard areas continues to intensify from the near-term to the long-term. The difference in the high-hazard regions between the mid-term and near-term periods is more pronounced than between the long-term and mid-term periods.

Figure 3b compares the global average drought hazard under different scenarios for the three future periods. In the near-term, drought hazard differs slightly among the four scenarios, with median values being slightly higher under SSP1-2.6 and SSP5-8.5. In the mid-term, drought hazard is similar under the four scenarios, with median values being slightly higher under SSP3-7.0 and SSP5-8.5. In the long-term, drought hazard is more significant under high and very high (GHG) emissions (SSP3-7.0 and SSP5-8.5) than other scenarios, especially under SSP5-8.5. Among all the different scenarios and periods, drought hazard shows the most significant increase in the long-term under SSP5-8.5 compared with the baseline period.

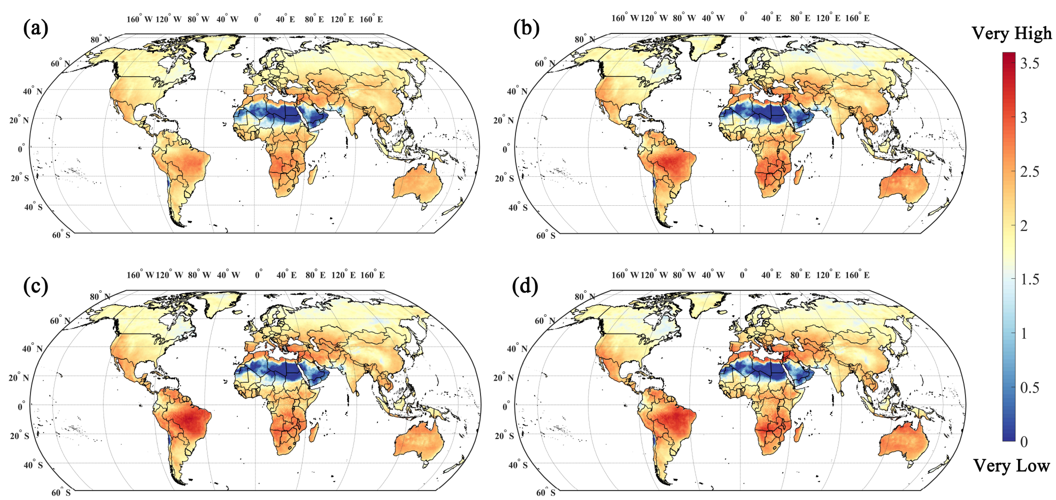

Figure 2. Distribution of the global drought hazard in (a) baseline period (1991–2014) and three projected periods: (b) 2021–2040, (c) 2041–2060, and (d) 2080–2100 under SSP2-4.5. SSP, shared socioeconomic pathway.

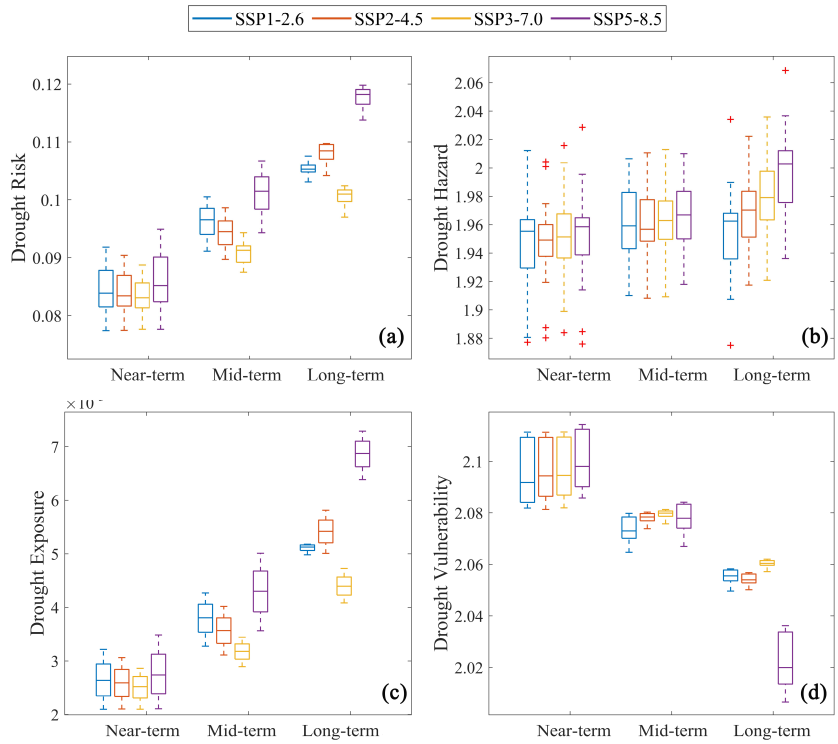

Figure 3. Global drought risk (a) and its three components of drought hazard (b), drought exposure (c), and drought vulnerability (d) in the near-term (2021–2040), mid-term (2041–2060), and long-term (2081–2100) under SSP1-2.6, SSP2-4.5, SSP3-7.0, and SSP5-8.5. SSP, shared socioeconomic pathway.

3.2. Spatiotemporal variation in drought exposure

Figure 4 shows the global distribution of drought exposure in the baseline period and the three projected periods under SSP2-4.5 (maps under the other three scenarios are provided in Figures S4–S6 in supplementary materials). Generally, the spatial distribution is relatively constant, and drought exposure varies widely worldwide. High exposure concentrates in India and southeastern China, with India showing the highest value (dark red scheme). Besides, drought exposure in Western Europe also maintains a relatively high level, especially in southern England, northern France, Netherlands, and northwestern Germany. So do the east and west coasts and state capitals in the United States. The worsening high exposure emerges in Africa, especially in southern Nigeria, northern Egypt, and central Ethiopia. Temporally, drought exposure gets significantly higher in the projected periods than the baseline period, especially in the high-exposed areas. Global average drought exposure shows an increasing trend over time under all scenarios (Figure 3c). In the near-term and mid-term, the increase is more significant in India and southeastern China compared to other regions. In the long-term, however, the greater increase is located in western and eastern Africa and India. Drought exposure in North America and Western Europe increases less pronouncedly.

Figure 3c compares the global average drought exposure under different scenarios in the three future periods. The differences among different scenarios are projected to get larger over time. Among the four SSPs, drought exposure is the highest under SSP5-8.5 and the lowest under SSP3-7.0 in all three future periods. Exposure under SSP1-2.6 is higher than that under SSP2-4.5 in the near-term and mid-term, while turning opposite in the long-term. The interquartile range of drought exposure values is minimal under SSP1-2.6 in the long-term.

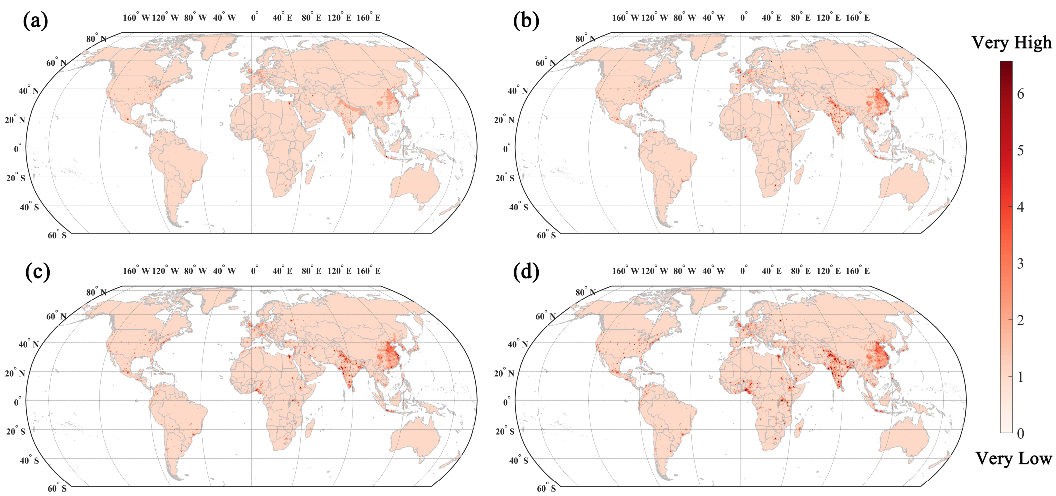

Figure 4. Distribution of the global drought exposure in (a) baseline period (1991–2014) and three projected periods: (b) 2021–2040, (c) 2041–2060, and (d) 2080–2100 under SSP2-4.5. SSP, shared socioeconomic pathway.

3.3. Spatiotemporal variation in drought vulnerability

Figure 5 shows the spatial distribution of drought vulnerability in the baseline period and the three projected periods under SSP2-4.5 (maps under the other three scenarios are provided in Figures S7–S9 in supplementary materials). The distributions are similar among different periods and scenarios with high vulnerability occurring in the regions covered with cropland and building land. High vulnerable regions and countries are eastern China, India, Southeastern Asia, Europe below 60°N latitude, western and eastern Africa, southern Australia, central and western United States, southern Mexico, and southeastern South America. Temporally, drought vulnerability in the projected periods is higher than in the baseline period, especially in the eastern United States, southern Brazil, eastern Argentina, southern Africa, and eastern China. Global average drought vulnerability shows a decreasing trend over time in the future under all scenarios (Figure 3d).

Figure 3d demonstrates the differences in drought vulnerability under various SSPs in the three future periods. Among the four scenarios, the decrease of drought vulnerability across time under SSP5-8.5 is projected to be the largest. In the near-term and mid-term, drought vulnerability is similar under the four SSPs, while significantly smaller under SSP5-8.5 than the other three scenarios in the long-term. In the mid-term and long-term, the interquartile ranges of drought vulnerability value are minimal under SSP2-4.5 and SSP3-7.0.

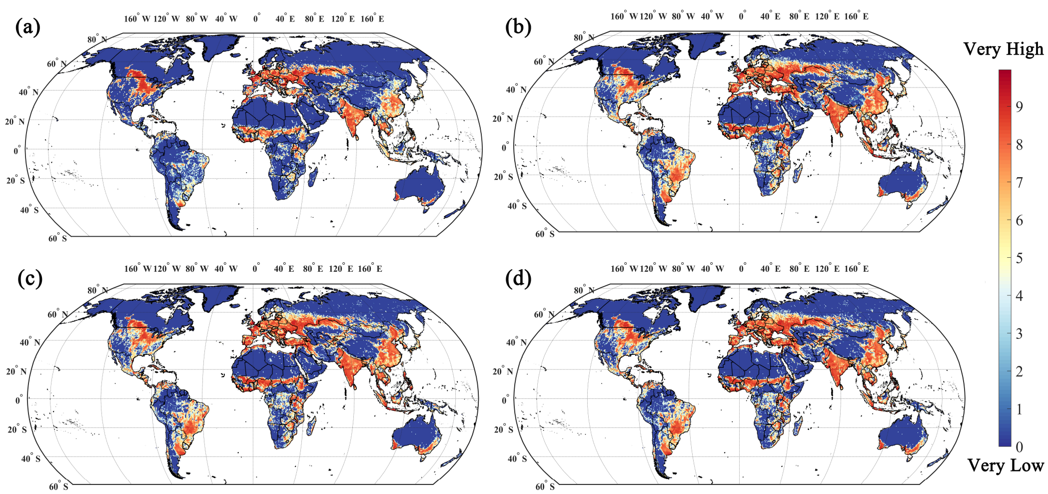

Figure 5. Distribution of the global drought vulnerability in (a) baseline period (1991–2014) and three projected periods: (b) 2021–2040, (c) 2041–2060, and (d) 2080–2100 under SSP2-4.5. SSP, shared socioeconomic pathway.

3.4. Future drought risk projection

3.4.1. Global drought risk map

Drought risk maps under SSP2-4.5 are shown in Figure 6 (maps under the other three scenarios are presented in Figures S10–S12 in supplementary materials). The raw risk values were classified into five grades using the natural breaks method (Basofi et al., 2015). The spatial distributions of drought risk are similar under the various scenarios and periods. The regions with high drought risk are concentrated in socially and economically developed areas. Sparsely populated regions demonstrated lower drought risk levels. The specific high-risk areas are (1) Africa: the Nile Delta from Cairo to Tanta in northern Egypt, Khartoum and its surrounding southern areas in Sudan, Addis Ababa and its surrounding areas in Ethiopia, Uganda, southern Kenya, southern Cote d'Ivoire, northern Morocco and Algeria, and the capital city of South Africa, Zambia, Congo; (2) Asia: southeastern China, especially the Pearl River Delta, Yangtze River delta, and the North China Plain; northern and southwestern India, northern Pakistan, western Syria, eastern Iraq, Manila in the Philippines, and Jakarta; (3) Austria: almost none region above level 4 with risk in the southeastern part relatively higher; (4) Europe: southern England, Netherlands, and big cities such as Paris, Berlin, Moscow, and their surrounding areas; (5) North America: southern Mexico and the eastern United States; and (6) South America: northern Colombia, northern Venezuela, and southern Brazil. The highest concentrations of high risk are in India and eastern China. In terms of temporal change, drought risk gets higher in the projected periods than the baseline period and keeps increasing in the future (Figure 3a). However, the rapid growth period differs spatially over the globe. From the near-term to the mid-term, drought risk increases faster in southeastern China, India, northern Egypt. From the mid-term to the long-term, drought risk increases faster in western and eastern Africa.

Figure 3a demonstrates the differences in drought risk under various SSPs in the three future periods. Among the four scenarios, drought risk is the highest under SSP5-8.5 in all the three future periods, followed by SSP1-2.6 and SSP2-4.5, and drought risk under SSP3-7.0 is the lowest. In addition, the differences in drought risk under different SSPs enlarger across time. The interquartile range of risk values in each period decreases from the near-term to the long-term.

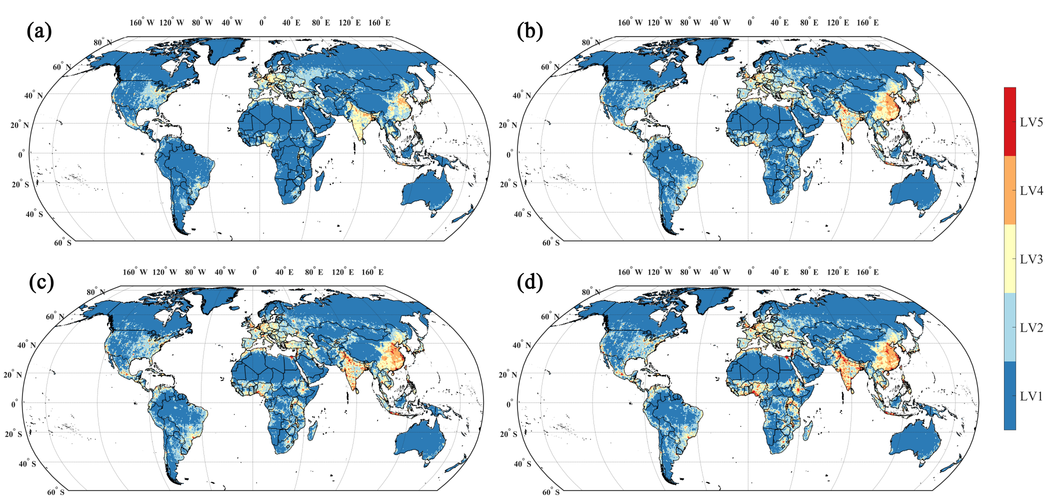

Figure 6. Distribution of the global drought risk in (a) baseline period (1991–2014) and three projected periods: (b) 2021–2040, (c) 2041–2060, and (d) 2080–2100 under SSP2-4.5. SSP, shared socioeconomic pathway; LV, level.

3.4.2. Continental drought risk projections

Figure 7 presents the temporal change of the spatial average drought risk under four SSPs for the six continents (excluding Antarctica). Drought risks for all six continents are projected to increase under the four scenarios. The highest average drought risk is observed in Europe, followed by Africa and Asia among the six continents. South America and North America rank fourth and fifth, respectively, and risk in Australia is the lowest. Africa has the most significant increase in drought risk, with the long-term period being almost three times greater than the baseline period under SSP5-8.5. From the baseline to the long-term period, the growth rates are about 60%, 60%, 45%, 70%, and 85% for Asia, Australia, Europe, North America, and South America under SSP5-8.5, respectively. Drought risk for Asia and South America increases more significantly from the baseline to the near-term period than from the near-term to the long-term period. In contrast, an opposite pattern is observed for Australia. The increase rates for other continents are relatively stable. Among the four SSPs, drought risk under SSP5-8.5 is the highest for all continents, while SSP3-7.0 is the lowest, and the difference between the two scenarios enlarges over time. Differences in drought risk between the four scenarios are significant in Australia, Europe, and North America, while much smaller in Africa, Asia, and South America. Drought risk under SSP1-2.6 is slightly higher than under SSP2-4.5 in the near-term, and the difference enlarges in the mid-term for all continents. In the long-term, drought risk under SSP2-4.5 turns out to be higher than SSP1-2.6 for Africa, Asia, Europe, and South America, while still lower than under SSP1-2.6 in Australia and North America.

Figure 8 shows the proportions of high drought risk grids (Level 4 and 5) for the six continents. The temporal changes are similar to the changes in the average drought risk (Figure 7) for all the continents under the four scenarios. Generally, the proportions of high-risk grids are more in Europe, Asia, and Africa. In the long-term, the upper quartile of proportion for Europe exceeds 10% under SSP5-8.5, with about 6% under SSP1-2.6 and SSP2-4.5 and 4% under SSP3-7.0. For Asia, the proportions under the four scenarios are relatively similar. The medians increase from 2% in the baseline period to about 5% in the near-term. Medians are 6% to 7% in the mid-term and 7% to 8% in the long-term. For Africa, the proportions of high-risk grids increase from 0.2% in the baseline period to around 5% in the long-term. The medians of high-risk proportion for North America and South America are close, and the highest values are about 2.2% in the long-term under

SSP5-8.5. High-risk grids proportions for Australia are the least, and the upper quartiles are always lower than 1% in all periods. Similar to the spatially average risk, the high-risk proportion under SSP5-8.5 is the highest among the four SSPs for all continents, while SSP3-7.0 is the lowest. The difference between the four scenarios increases over time, especially in Australia, Europe, and North America. The proportions under SSP1-2.6 and SSP2-4.5 are close for all six continents in the near-term. However, in the mid-term, the high-risk proportion under SSP1-2.6 is higher than that under SSP2-4.5, especially for Africa and South America. On the contrary, the high-risk proportion under SSP2-4.5 is higher than SSP1-2.6 in the long-term for all continents except Australia.

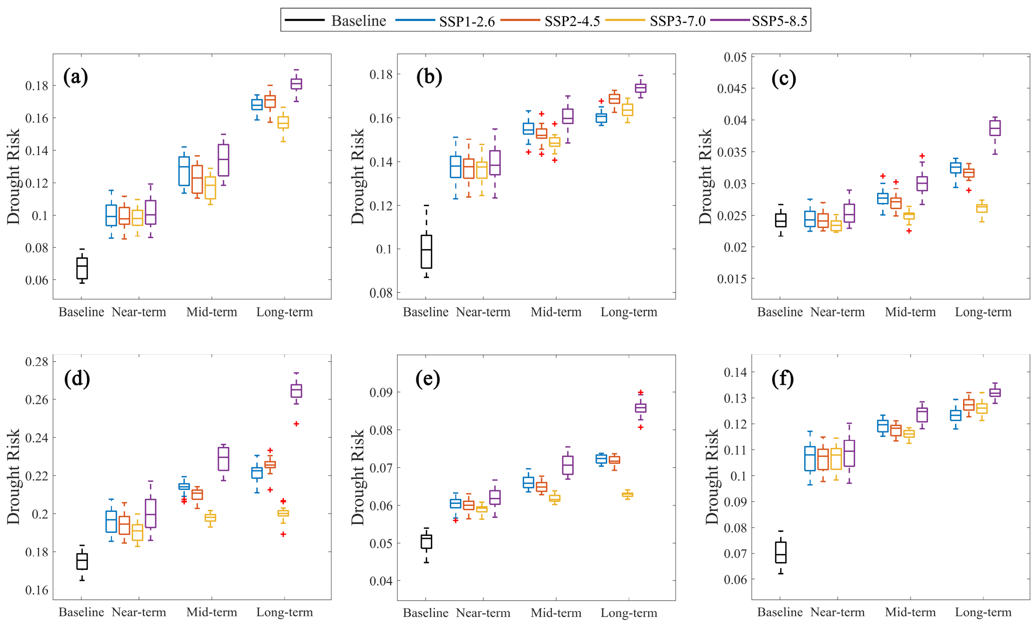

Figure 7. Spatial drought risk of (a) Africa, (b) Asia, (c) Australia, (d) Europe, (e) North America, and (f) South America in the baseline period (1991-2014), near-term (2021–2040), mid-term (2041–2060), and long-term (2080–2100) under SSP1-2.6, SSP2-4.5, SSP3-7.0, and SSP5-8.5. SSP, shared socio-economic pathway.

Figure 8. The proportion of grids with drought risk above Level 3 for (a) Africa, (b) Asia, (c) Australia, (d) Europe, (e) North America, and (f) South America in the baseline period (1991-2014), near-term (2021–2040), mid-term (2041–2060), and long-term (2080–2100) under SSP1-2.6, SSP2-4.5, SSP3-7.0, and SSP5-8.5. SSP, shared socioeconomic pathway.

3.4.3. Continental population and GDP under high drought risk

We counted the population and GDP at high drought risk (above Level 3, Figure 9 and Figure 10) and the highest drought risk (Level 5, Figure S13 and Figure S14 in supplementary materials) for the six continents in the baseline period and three projected periods under four SSPs. Figure 9 shows that the total populations under high and the highest drought risk both increase in the projected periods than the baseline period for all the six continents. Among the six continents, populations under high and the highest risk for Asia are both the largest, with the maximum values reaching 5 billion and almost 3 billion in the long-term under SSP3-7.0. Africa is the second largest with the medians of more than 2 and 1.3 billion under high and the highest risk in the long-term under SSP3-7.0. In addition, Africa has the most significant increase in population under high and the highest risk. The total populations under high and the highest drought risk for Europe and North America are close, reaching about 600 and over 300 billion in the long-term under SSP5-8.5. Comparing the four scenarios, the total populations under high risk are similar in the near-term. However, the differences among the different SSPs enlarge in the mid-term and long-term. For Africa, Asia, and South America, the total population under high risk is the largest under SSP3-7.0, followed by SSP2-4.5, and similar under the other two SSPs. For Australia, Europe, and North America, the total population under high risk is the largest under SSP5-8.5 with the lowest under SSP3-7.0, and the values are similar under SSP1-2.6 and SSP2-4.5. Under the highest risk, the relative population size among the four scenarios is consistent with the high risk for all six continents.

Figure 10 shows the total GDPs under high and the highest drought risk keep increasing for all continents. Similar to the population, the most significant increases in GDP under high and the highest risk both occur in Africa, with the median of the total GDP under high drought risk reaching 100 trillion US dollars (2010 price) under SSP5-8.5 in the long-term. The values under the highest risk are about 2/3 as high risk. The total GDPs under high and the highest drought risk are both the largest for Asia, with the median over 350 and 200 trillion, respectively. GDPs under high drought risk for Europe and North America are close, and Australia is the smallest. Comparing the four scenarios, the total GDPs under high risk are similar in the near-term, and the differences among the different SSPs enlarge in the mid-term and long-term. The total GDP exposed to high risk is the largest under SSP5-8.5 and the smallest under SSP3-7.0 for all continents. The values are similar under SSP1-2.6 and SSP2-4.5. The differences between the SSP5-8.5 and other SSPs are significant for Australia, Europe, and North America. Under the highest risk, the relative GDP size among the four scenarios is consistent with the high risk for all six continents.

Figure 9. The total population under drought risk above Level 3 for (a) Africa, (b) Asia, (c) Australia,

(d) Europe, (e) North America, and (f) South America in the baseline period (1991-2014), near-term (2021–2040), mid-term (2041–2060), and long-term (2080–2100) under SSP1-2.6, SSP2-4.5, SSP3-7.0, and SSP5-8.5. SSP, shared socioeconomic pathway.

Figure 10. The total GDP under drought risk above Level 3 for (a) Africa, (b) Asia, (c) Australia, (d) Europe, (e) North America, and (f) South America in the baseline period (1991-2014), near-term (2021–2040), mid-term (2041–2060), and long-term (2080–2100) under SSP1-2.6, SSP2-4.5, SSP3-7.0, and SSP5-8.5. GDP, Gross Domestic Product; SSP, shared socioeconomic pathway.

4. Discussion

This study presents the future global drought risk map under SSP1-2.6, SSP2-4.5, SSP3-7.0, and SSP5-8.5, combining hazard, exposure, and vulnerability. Drought risk for the six continents and their population and GDP under high drought risk is specifically analyzed. The results show that high drought hazard areas are mainly distributed in central Brazil, southwestern North America, northern and southern Africa, southern Europe, southwestern Asia, and Australia, which is generally consistent with the drought-prone areas in the previous studies (Carrao et al., 2016; Li et al., 2021; Lu et al., 2019). However, drought hazard in central Brazil and North America is higher herein than in some previous studies (Carrao et al., 2016; Wang et al., 2021). Such differences may arise from the selection of drought indexes and meteorological data from different sources. We used 3-ten-days SPI to identify drought, and thus more short droughts were identified. When examining the temporal change, the global average drought hazard shows an increasing trend in the future, especially under SSP5-8.5, which is similar to the previous findings (Li et al., 2021).

In the exposure analysis, drought exposure is significantly higher in the developed areas and increases significantly in the future. Among the four SSPs, drought exposure is the highest under SSP5-8.5 and the lowest under SSP3-7.0. In addition, we found that exposure values under SSP1-2.6 in the long-term are concentrated, implying that drought exposure may reach a peak and stop growing after 2080 under SSP1-2.6. Vulnerability assessment is complicated since it reflects the adaption and sensitivity levels of the social system to drought. In this study, ratios of the cropland and built-up land, road density, and channel density were chosen to reflect the agricultural and infrastructure factors and water resource conditions. In addition, we used the GDP per capita to represent the resistance to drought disasters. The high vulnerable regions are observed in eastern China, India, Southeastern Asia, Western Europe, western and eastern Africa, southern Australia, central and western United States, southern Mexico, and southeastern South America. These are places where cultivated land and human settlements are concentrated. The distribution is similar to previous studies (Carrao et al., 2016; Y. J. Liu & Chen, 2021), while several differences exist due to the selection of indicators. Global average drought vulnerability shows a decreasing trend over time in the future since the GDP per capita increases significantly. In the mid-term and long-term, the interquartile range of drought vulnerability values are very small under SSP2-4.5 and SSP3-7.0, showing that drought vulnerability may stop decreasing and maintain stability after 2040 under these two scenarios.

As revealed in this study, the high drought risk regions are mainly distributed in the areas with high exposure, which is consistent with the previous studies (Carrao et al., 2016; Y. J. Liu & Chen, 2021). In the future, consistent with other studies (Ahmadalipour et al., 2019; Song et al., 2021; Q. Zhang et al., 2019), average drought risk and high risk are projected to keep increasing. Among the four SSPs, drought risk is the highest under SSP5-8.5, followed by SSP1-2.6, SSP2-4.5, and SSP3-7.0, while in some studies the order may be different due to the different combinations of the SSPs and RCPs. However, it is consistent that the drought risk is higher under the scenarios with high greenhouse gas emissions and more population and GDP (Ahmadalipour et al., 2019; Y. J. Liu & Chen, 2021). In addition, the interquartile range of risk values in each period decreases from the near-term to the long-term, showing that the growth rate of drought risk decreases over time, which is consistent with other findings (Ahmadalipour et al., 2019;

Mondal et al., 2021).

To better understand the drought risk for the continents, we counted the drought risk at continental scale. Among the six continents, the highest average drought risk and ratios of high drought risk grids are in Europe, followed by Asia and Africa, resulting from the high proportions of urbanization and cropland. Risk is the highest under SSP5-8.5 and lowest under SSP3-7.0 for all continents, and the difference is more significant for Europe, North America, and Australia. That is because population and GDP vary more largely under different SSPs for the three developed continents in the long-term than the less developed continents. The population and GDP under high risk for each continent remind that more attention should be paid to countries in Asia and Africa because of their vast amount and rapid increases in the social economy. Among the four SSPs, the population under high risk for the less developed continents (Africa, Asia, and South America) is the largest under SSP3-7.0, with being the lowest under this scenario for the other three continents. The reason is that the SSP3-7.0 is a scenario of an imbalanced developed and regionally differentiated world, with faster population growth in developing countries, constrained by educational and technological development. The population under high risk for the relatively well-developed continents (Europe, North America, and South America) is the largest under SSP5-8.5 among different SSP, likely due to the population migration to socioeconomically developed areas. For GDP, differences between the SSP5-8.5 and other SSPs are more significant for Australia, Europe, and North America. These differences among the developed and less developed continents may result from spatial development inequality under different SSPs. The largest increases in population and GDP under high drought risk both occur in Africa, reminding that effective drought hazard adaptation measures are in urgent need to be taken to enable socioeconomic systems in Africa.

There are some limitations in this study due to uncertainties during the assessment process, including the uncertainties in the choice of indicators and uncertainties in the indicator data. On the one hand, the indicators can be more diverse and comprehensive when the data are available. In hazard analysis, other drought indices such as the Palmer drought severity index (Palmer, 1965) and the standardized precipitation evapotranspiration index (Vicente-Serrano et al., 2010) can also be used. In exposure and vulnerability assessment, other socioeconomic factors that influence exposure and vulnerability, such as the age/sex structure and the industrial structure should also be considered. In addition, the density and volume of the reservoirs should be taken into account as the drought disaster reduction ability. Different indicators may result in inconsistent results (Yao et al., 2018; X. Zhang et al., 2017). On the other hand, there are uncertainties in selecting GCMs and projections of population, GDP, and land use. Climate models are also subject to significant uncertainty (Monerie et al., 2020; Tabari et al., 2019). Nevertheless, in this study, bias corrections have been conducted to improve the GCMs outputs, and the projections of socioeconomic data were simulated under different SSP scenarios. In addition, uncertainty exists in all studies on future projections that cannot be avoided entirely (Q. Yin et al., 2019). Therefore, the results of this study can be considered to be reasonable. In further studies, more comprehensive assessment models can be used to predict drought risk by combining more accurate available data with higher resolution.

5. Conclusion

We assessed and predicted global drought risk under various SSP-RCP scenarios by adopting the risk quantification formula proposed by IPCC and selecting evaluation indicators of hazard, exposure, and vulnerability. Three key findings are summarized as follows.

(1) High drought risk areas are mainly distributed in southeastern China, India, Western Europe, eastern United States, and western and eastern Africa. Global drought risk gets higher in the projected periods than the baseline period and keeps increasing in the future. Among the four SSPs, the highest and lowest drought risk would be under SSP5-8.5 and SSP3-7.0, respectively.

(2) Averaged drought risk and high risk for all six continents are projected to increase under the four scenarios. Europe, Asia, and Africa are projected to be the continents with higher average risk and more high-risk grids among the six continents. Among the four SSPs, drought risk under SSP5-8.5 is the highest for all continents, while SSP3-7.0 is the lowest.

(3) Populations under high drought risk for Asia and Africa are much more massive than other continents, with being the most for Asia. For Africa, Asia, and South America, the total populations exposed to high risk are the largest under SSP3-7.0, followed by SSP2-4.5 and similar under SSP1-2.6 and SSP5-8.5. For Australia, Europe, and North America, the total populations exposed to high risk are the largest under SSP5-8.5 with the smallest under SSP3-7.0, and the values are similar under SSP1-2.6 and SSP2-4.5. GDP under high drought risk in Asia is the highest among the six continents. Among the

four scenarios, the total GDP under high risk is the largest under SSP5-8.5 and the smallest under SSP3-7.0 for all continents, with being similar under SSP1-2.6 and SSP2-4.5. The most significant increases in population and GDP under high drought risk both occur in Africa.

Overall, the findings of this study highlight the relative sensitivity of socioeconomic drought risk to different SSP-RCP scenarios across the globe. Our research can be a bridge between physical and social sciences to help policymakers develop effective adaptive techniques to enhance drought resilience.

Acknowledgments

This work is supported by the National Key Research and Development Program of China (No.2017YFA0603704). We also acknowledge support by Major projects of the National Natural Science Foundation of China (No.41890824) and the Excellent Young Scientists Fund, and the Strategic Priority Research Program of the Chinese Academy of Sciences (No. XDA23040500).

Author contributions

LPZ conceived the original idea, and ZLZ designed the methodology. LPZ, JC, and YJZ collected the data. ZLZ developed the code and performed the analysis, with some contributions from QZ and DXS. ZLZ, LPZ, JC, and DXS contributed to the interpretation of results. ZLZ wrote the first version of the manuscript, and LPZ, JC, GSW, and JX revised the paper.

Data availability

The climate simulation data can be accessed from the CMIP6 archive (https://esgf-node.llnl.gov/projects/cmip6/). The observation climate data during can be accessed from National Oceanic and Atmospheric Administration (NOAA) Physical Sciences Laboratory (https://psl.noaa.gov/data/gridded/index.html). Global annual 1 km population data during 2000 to 2014 can be accessed from WorldPop archive (https://www.worldpop.org/geodata/listing?id=64). Global 1 km population data in 1990, 1995, and 2000 can be accessed from Socioeconomic Data and Applications Center (SEDAC) (https://sedac.ciesin.columbia.edu/data/collection/grump-v1). Global annual 5 arc-min GDP data during 1991 to 2014 can be accessed from Dryad Data (https://datadryad.org/stash/dataset/doi:10.5061/dryad.dk1j0). Projected 0.5° gridded global population and GDP data can be accessed from figshare (https://figshare.com/s/5433bdfcb503fbac8303). Global annual 300m land cover data during 1991 to 2014 can be gained from European Space Agency (ESA, https://www.esa-landcover-cci.org/?q=node/197). Global 0.1° × 0.1° land cover projections can be gained from figshare (https://figshare.com/s/ace7581c0863241ac5e1). Global road density data can be accessed from the Global Roads Inventory Project (GRIP) dataset (https://www.globio.info/download-grip-dataset). Global river network data can be gained from figshare (https://figshare.com/articles/dataset/A_data_set_of_global_river_networks_and_corresponding_water_resources_zones_divisions/8044184/6).

Conflict of interest

The authors declare that they have no conflict of interest with the work presented here.

References

Ahmadalipour, A., Moradkhani, H., Castelletti, A., & Magliocca, N. (2019). Future drought risk in Africa: Integrating vulnerability, climate change, and population growth. *Science of the Total Environment*, *662*, 672–686. https://doi.org/10.1016/j.scitotenv.2019.01.278

Ayugi, B., Zhihong, J., Zhu, H. H., Ngoma, H., Babaousmail, H., Rizwan, K., & Dike, V. (2021). Comparison of CMIP6 and CMIP5 models in simulating mean and extreme precipitation over East Africa. *International Journal of Climatology*, *41*(15), 6474–6496. https://doi.org/10.1002/joc.7207

Balk, D. L., Deichmann, U., Yetman, G., Pozzi, F., Hay, S. I., & Nelson, A. (2006). Determining Global Population Distribution: Methods, Applications and Data. *Advances in Parasitology*, *62*, 119–156. Retrieved from https://doi.org/10.1016/S0065-308X(05)62004-0

Cai, W. J., Cowan, T., Briggs, P., & Raupach, M. (2009). Rising temperature depletes soil moisture and exacerbates severe drought conditions across southeast Australia. *Geophysical Research Letters*, *36*. https://doi.org/10.1029/2009gl040334

Carrao, H., Naumann, G., & Barbosa, P. (2016). Mapping global patterns of drought risk: An empirical framework based on sub-national estimates of hazard, exposure and vulnerability. *Global Environmental Change-Human and Policy Dimensions*, *39*, 108–124. https://doi.org/10.1016/j.gloenvcha.2016.04.012

Center for International Earth Science Information Network - CIESIN - Columbia University, International Food Policy Research Institute - IFPRI, The World Bank, & Centro Internacional de Agricultura Tropical - CIAT. (2011). Global Rural-Urban Mapping Project, Version 1 (GRUMPv1) [Dataset]: Population Count Grid. Palisades, NY: NASA Socioeconomic Data and Applications Center (SEDAC). https://doi.org/10.7927/H4VT1Q1H

Chou, J. M., Xian, T., Zhao, R. Z., Xu, Y., Yang, F., & Sun, M. Y. (2019). Drought Risk Assessment and Estimation in Vulnerable Eco-Regions of China: Under the Background of Climate Change. *Sustainability*, *11*(16). https://doi.org/10.3390/su11164463

Cook, B. I., Mankin, J. S., Marvel, K., Williams, A. P., Smerdon, J. E., & Anchukaitis, K. J. (2020). Twenty-First Century Drought Projections in the CMIP6 Forcing Scenarios. *Earths Future*, *8*(6). https://doi.org/10.1029/2019ef001461

Dabanli, I., Mishra, A. K., & Sen, Z. (2017). Long-term spatio-temporal drought variability in Turkey. *Journal of Hydrology*, *552*, 779–792. https://doi.org/10.1016/j.jhydrol.2017.07.038

Dai, M., Huang, S. Z., Huang, Q., Leng, G. Y., Guo, Y., Wang, L., et al. (2020). Assessing agricultural drought risk and its dynamic evolution characteristics. *Agricultural Water Management*, *231*. https://doi.org/10.1016/j.agwat.2020.106003

Dashtpagerdi, M. M., Kousari, M. R., Vagharfard, H., Ghonchepour, D., Hosseini, M. E., & Ahani, H. (2015). An investigation of drought magnitude trend during 1975-2005 in arid and semi-arid regions of Iran. *Environmental Earth Sciences*, *73*(3), 1231–1244. https://doi.org/10.1007/s12665-014-3477-1

Dong, T. Y., & Dong, W. J. (2021). Evaluation of extreme precipitation over Asia in CMIP6 models. *Climate Dynamics*, *57*(7–8), 1751–1769. https://doi.org/10.1007/s00382-021-05773-1

Fan, Z. M., Li, J., & Yue, T. X. (2013). Land-cover changes of biome transition zones in Loess Plateau of China. *Ecological Modelling*, *252*, 129–140. https://doi.org/10.1016/j.ecolmodel.2012.07.039

Fan, Z. M., Li, J., Yue, T. X., Zhou, X., & Lan, A. J. (2015). Scenarios of land cover in

Karst area of Southwestern China. *Environmental Earth Sciences*, *74*(8), 6407–6420. https://doi.org/10.1007/s12665-015-4223-z

Fan, Z. M., Li, S. B., & Fang, H. Y. (2020). Explicitly Identifying the Desertification Change in CMREC Area Based on Multisource Remote Data. *Remote Sensing*, *12*(19). https://doi.org/10.3390/rs12193170

Fan, Z. M., Bai, R. Y., & Yue, T. X. (2020). Scenarios of land cover in Eurasia under climate change. *Journal of Geographical Sciences*, *30*(1), 3–17. https://doi.org/10.1007/s11442-020-1711-1

Guo, H., Wang, R., Garfin, G. M., Zhang, A. Y., Lin, D. G., Liang, Q. O., & Wang, J. A. (2021). Rice drought risk assessment under climate change: Based on physical vulnerability a quantitative assessment method. *Science of the Total Environment*, *751*. https://doi.org/10.1016/j.scitotenv.2020.141481

Guttman, N. B. (1999). Accepting the standardized precipitation index: A calculation algorithm. *Journal of the American Water Resources Association*, *35*(2), 311–322. https://doi.org/10.1111/j.1752-1688.1999.tb03592.x

Hoque, M. A., Pradhan, B., & Ahmed, N. (2020). Assessing drought vulnerability using geospatial techniques in northwestern part of Bangladesh. *Science of the Total Environment*, *705*. https://doi.org/10.1016/j.scitotenv.2019.135957

Hoque, M. A. A., Pradhan, B., Ahmed, N., & Sohel, M. S. I. (2021). Agricultural drought risk assessment of Northern New South Wales, Australia using geospatial techniques. *Science of the Total Environment*, *756*. https://doi.org/10.1016/j.scitotenv.2020.143600

Huang, J. L., Qin, D. H., Jiang, T., Wang, Y. J., Feng, Z. Q., Zhai, J. Q., et al. (2019). Effect of Fertility Policy Changes on the Population Structure and Economy of China: From the Perspective of the Shared Socioeconomic Pathways. *Earths Future*, *7*(3), 250–265. https://doi.org/10.1029/2018ef000964

IPCC. (2012). *Managing the risks of extreme events and disasters to advance climate change adaptation: special report of the intergovernmental panel on climate change* [Field, C.B., V. Barros, T.F. Stocker, D. Qin, D.J. Dokken, K.L. Ebi, M.D. Mastrandrea, K.J. Mach, G.-K. Plattner, S.K. Allen, M. Tignor, and P.M. Midgley (eds.)]. Cambridge, UK and New York, USA: Cambridge University Press.

IPCC. (2014). *Climate Change 2014: Synthesis Report. Contribution of Working Groups I, II and III to the Fifth Assessment Report of the Intergovernmental Panel on Climate Change* [Core Writing Team, R.K. Pachauri and L.A. Meyer (eds.)]. Cambridge, UK and New York, USA: Cambridge University Press.

IPCC. (2021). *Summary for Policymakers. In: Climate Change 2021: The Physical Science Basis. Contribution of Working Group I to the Sixth Assessment Report of the Intergovernmental Panel on Climate Change* [Masson-Delmotte, V., P. Zhai, A. Pirani, S. L. Connors, C. Péan, S. Berger, N. Caud, Y. Chen, L. Goldfarb, M. I. Gomis, M. Huang, K. Leitzell, E. Lonnoy, J.B.R. Matthews, T. K. Maycock, T. Waterfield, O. Yelekçi, R. Yu and B. Zhou (eds.)]. Cambridge, UK and New York, USA: Cambridge University Press. In Press.

ISFD Reduction. (2004). *Living with risk: a global review of disaster reduction initiatives*. Geneva, CH: United Nations Publications.

Jiang, T., Zhao, J., Cao, L., Wang, Y., Su, B., Jing, C., et al. (2018). Projection of national and provincial economy under the shared socioeconomic pathways in China. *Progressus Inquisitiones de Mutatione Climatis*, *14*(1), 50–58.

Jiang, T., Wang, Y., Yuan, J., Chen, Y., Gao, X., Jing, C., et al. (2018). Projection of population and economy in the Belt and Road countries (2020-2060). *Progressus Inquisitiones de Mutatione Climatis*, *14*(2), 155–164.

Jing, C., Tao, H., Jiang, T., Wang, Y. J., Zhai, J. Q., Cao, L. G., & Su, B. D. (2020). Population, urbanization and economic scenarios over the Belt and Road region under the Shared Socioeconomic Pathways. *Journal of Geographical Sciences*, *30*(1), 68–84. https://doi.org/10.1007/s11442-020-1715-x

Khoshnazar, A., Perez, G. A. C., & Diaz, V. (2021). Spatiotemporal Drought Risk Assessment Considering Resilience and Heterogeneous Vulnerability Factors: Lempa Transboundary River Basin in The Central American Dry Corridor. *Journal of Marine Science and Engineering*, *9*(4). https://doi.org/10.3390/jmse9040386

Kim, J. S., Park, S. Y., Hong, H. P., Chen, J., Choi, S. J., Kim, T. W., & Lee, J. H. (2020). Drought risk assessment for future climate projections in the Nakdong River Basin, Korea. *International Journal of Climatology*, *40*(10), 4528–4540. https://doi.org/10.1002/joc.6473

Kummu, M., Taka, M., & Guillaume, J. H. A. (2018). Data Descriptor: Gridded global datasets for Gross Domestic Product and Human Development Index over 1990-2015. *Scientific Data*, *5*. https://doi.org/10.1038/sdata.2018.4

Le, T., Sun, C., Choy, S., & Kuleshov, Y. (2021). Regional drought risk assessment in the Central Highlands and the South of Vietnam. *Geomatics Natural Hazards & Risk*, *12*(1), 3140–3159. https://doi.org/10.1080/19475705.2021.1998232

Lehner, F., Coats, S., Stocker, T. F., Pendergrass, A. G., Sanderson, B. M., Raible, C. C., & Smerdon, J. E. (2017). Projected drought risk in 1.5 degrees C and 2 degrees C warmer climates. *Geophysical Research Letters*, *44*(14), 7419–7428. https://doi.org/10.1002/2017gl074117

Lesk, C., Rowhani, P., & Ramankutty, N. (2016). Influence of extreme weather disasters on global crop production. *Nature*, *529*(7584), 84-+. https://doi.org/10.1038/nature16467

Li, H. W., Li, Z., Chen, Y. N., Xiang, Y. Y., Liu, Y. C., Kayumba, P. M., & Li, X. Y. (2021). Drylands face potential threat of robust drought in the CMIP6 SSPs scenarios. *Environmental Research Letters*, *16*(11). https://doi.org/10.1088/1748-9326/ac2bce

Liu, X., Guo, P., Tan, Q., Zhang, F., Huang, Y., & Wang, Y. Z. (2021). Drought disaster risk management based on optimal allocation of water resources. *Natural Hazards*, *108*(1), 285–308. https://doi.org/10.1007/s11069-021-04680-2

Liu, Y. J., & Chen, J. (2021). Future global socioeconomic risk to droughts based on estimates of hazard, exposure, and vulnerability in a changing climate. *Science of the Total Environment*, *751*. https://doi.org/10.1016/j.scitotenv.2020.142159

Lloyd, C. T., Chamberlain, H., Kerr, D., Yetman, G., Pistolesi, L., Stevens, F. R., et al. (2019). Global spatio-temporally harmonised datasets for producing high-resolution gridded population distribution datasets. *Big Earth Data*, *3*(2), 108–139. https://doi.org/10.1080/20964471.2019.1625151

Lu, Y. J., Cai, H. J., Jiang, T. T., Sun, S. K., Wang, Y. B., Zhao, J. F., et al. (2019). Assessment of global drought propensity and its impacts on agricultural water use in future climate scenarios. *Agricultural and Forest Meteorology*, *278*. https://doi.org/10.1016/j.agrformet.2019.107623

Marengo, J. A., Torres, R. R., & Alves, L. M. (2017). Drought in Northeast Brazil-past, present, and future. *Theoretical and Applied Climatology*, *129*(3–4), 1189–1200. https://doi.org/10.1007/s00704-016-1840-8

McKee, T. B., Doesken, N. J., & Kleist, J. (1993). The relationship of drought frequency and duration to time scales. In *Proceedings of the 8th Conference on Applied Climatology* (Vol. 17, pp. 179–183). Boston.

Meijer, J. R., Huijbregts, M. A. J., Schotten, K., & Schipper, A. M. (2018). Global patterns of current and future road infrastructure. *Environmental Research Letters*, *13*(6). https://doi.org/10.1088/1748-9326/aabd42

Meza, I., Siebert, S., Doll, P., Kusche, J., Herbert, C., Rezaei, E. E., et al. (2020). Global-scale drought risk assessment for agricultural systems. *Natural Hazards and Earth System Sciences*, *20*(2), 695–712. https://doi.org/10.5194/nhess-20-695-2020

Mokarram, M., Pourghasemi, H. R., Hu, M., & Zhang, H. C. (2021). Determining and forecasting drought susceptibility in southwestern Iran using multi-criteria decision-making (MCDM) coupled with CA-Markov model. *Science of the Total Environment*, *781*. https://doi.org/10.1016/j.scitotenv.2021.146703

Mondal, S. K., Huang, J. L., Wang, Y. J., Su, B. D., Zhai, J. Q., Tao, H., et al. (2021). Doubling of the population exposed to drought over South Asia: CMIP6 multi-model-based analysis. *Science of the Total Environment*, *771*. https://doi.org/10.1016/j.scitotenv.2021.145186

Monerie, P. A., Wainwright, C. M., Sidibe, M., & Akinsanola, A. A. (2020). Model uncertainties in climate change impacts on Sahel precipitation in ensembles of CMIP5 and CMIP6 simulations. *Climate Dynamics*, *55*(5–6), 1385–1401. https://doi.org/10.1007/s00382-020-05332-0

Naumann, G., Alfieri, L., Wyser, K., Mentaschi, L., Betts, R. A., Carrao, H., et al. (2018). Global Changes in Drought Conditions Under Different Levels of Warming. *Geophysical Research Letters*, *45*(7), 3285–3296. https://doi.org/10.1002/2017gl076521

O'Neill, B. C., Tebaldi, C., van Vuuren, D. P., Eyring, V., Friedlingstein, P., Hurtt, G., et al. (2016). The Scenario Model Intercomparison Project (ScenarioMIP) for CMIP6. *Geoscientific Model Development*, *9*(9), 3461–3482. https://doi.org/10.5194/gmd-9-3461-2016

OECD. (2008). *Handbook on constructing composite indicators: methodology and user guide*. Paris, FR: OECD publishing.

Palchaudhuri, M., & Biswas, S. (2016). Application of AHP with GIS in drought risk assessment for Puruliya district, India. *Natural Hazards*, *84*(3), 1905–1920. https://doi.org/10.1007/s11069-016-2526-3

Palmer, W. C. (1965). *Meteorological drought* (Vol. 30). Washington, DC: US Department of Commerce, Weather Bureau.

Pearson, L., & Pelling, M. (2015). The UN Sendai framework for disaster risk reduction 2015–2030: Negotiation process and prospects for science and practice. *Journal of Extreme Events*, *2*(01), 1571001.

Peduzzi, P., Dao, H., Herold, C., & Mouton, F. (2009). Assessing global exposure and vulnerability towards natural hazards: the Disaster Risk Index. *Natural Hazards and Earth System Sciences*, *9*(4), 1149–1159. https://doi.org/10.5194/nhess-9-1149-2009

Prabnakorn, S., Maskey, S., Suryadi, F. X., & de Fraiture, C. (2019). Assessment of drought hazard, exposure, vulnerability, and risk for rice cultivation in the Mun River Basin in Thailand. *Natural Hazards*, *97*(2), 891–911. https://doi.org/10.1007/s11069-019-03681-6

Riahi, K., van Vuuren, D. P., Kriegler, E., Edmonds, J., O'Neill, B. C., Fujimori, S., et al. (2017). The Shared Socioeconomic Pathways and their energy, land use, and greenhouse gas emissions implications: An overview. *Global Environmental Change-Human and Policy Dimensions*, *42*, 153–168. https://doi.org/10.1016/j.gloenvcha.2016.05.009

Saaty, T. L., & Vargas, L. G. (2001). Models, methods, concepts & applications of the analytic hierarchy process. *International Series in Operations Research and Management Science*. https://doi.org/10.1007/978-1-4615-1665-1

Saaty, T. L. (1987). Rank generation, preservation, and reversal in the analytic hierarchy decision process. *Decision Sciences*, *18*(2), 157–177. https://doi.org/10.1111/j.1540-5915.1987.tb01514.x

Sahana, V., Mondal, A., & Sreekumar, P. (2021). Drought vulnerability and risk assessment in India: Sensitivity analysis and comparison of aggregation techniques. *Journal of Environmental Management*, *299*. https://doi.org/10.1016/j.jenvman.2021.113689

Sian, K., Wang, J. H., Ayugi, B. O., Nooni, I. K., & Ongoma, V. (2021). Multi-Decadal Variability and Future Changes in Precipitation over Southern Africa. *Atmosphere*, *12*(6). https://doi.org/10.3390/atmos12060742

Song, Y. L., Tian, J. F., Linderholm, H. W., Wang, C. Y., Ou, Z. R., & Chen, D. L. (2021). The contributions of climate change and production area expansion to drought risk for maize in China over the last four decades. *International Journal of Climatology*, *41*, E2851–E2862. https://doi.org/10.1002/joc.6885

Spinoni, J., Naumann, G., Carrao, H., Barbosa, P., & Vogt, J. (2014). World drought frequency, duration, and severity for 1951-2010. *International Journal of Climatology*, *34*(8), 2792–2804. https://doi.org/10.1002/joc.3875

Spinoni, J., Vogt, J. V, Naumann, G., Barbosa, P., & Dosio, A. (2018). Will drought events become more frequent and severe in Europe? *International Journal of*

Climatology, *38*(4), 1718–1736. https://doi.org/10.1002/joc.5291

Su, B. D., Huang, J. L., Fischer, T., Wang, Y. J., Kundzewicz, Z. W., Zhai, J. Q., et al. (2018). Drought losses in China might double between the 1.5 degrees C and 2.0 degrees C warming. *Proceedings of the National Academy of Sciences of the United States of America*, *115*(42), 10600–10605. https://doi.org/10.1073/pnas.1802129115

Su, B. D., Huang, J. L., Mondal, S. K., Zhai, J. Q., Wang, Y. J., Wen, S. S., et al. (2021). Insight from CMIP6 SSP-RCP scenarios for future drought characteristics in China. *Atmospheric Research*, *250*. https://doi.org/10.1016/j.atmosres.2020.105375

Sun, Z. Y., Zhang, J. Q., Zhang, Q., Hu, Y., Yan, D. H., & Wang, C. Y. (2014). Integrated risk zoning of drought and waterlogging disasters based on fuzzy comprehensive evaluation in Anhui Province, China. *Natural Hazards*, *71*(3), 1639–1657. https://doi.org/10.1007/s11069-013-0971-9

Tabari, H., Hosseinzadehtalaei, P., AghaKouchak, A., & Willems, P. (2019). Latitudinal heterogeneity and hotspots of uncertainty in projected extreme precipitation. *Environmental Research Letters*, *14*(12). https://doi.org/10.1088/1748-9326/ab55fd

Takeshima, A., Kim, H., Shiogama, H., Lierhammer, L., Scinocca, J. F., Seland, O., & Mitchell, D. (2020). Global aridity changes due to differences in surface energy and water balance between 1.5 degrees C and 2 degrees C warming. *Environmental Research Letters*, *15*(9). https://doi.org/10.1088/1748-9326/ab9db3

Tang, B., Hu, W. T., & Duan, A. M. (2021). Assessment of Extreme Precipitation Indices over Indochina and South China in CMIP6 Models. *Journal of Climate*, *34*(18), 7507–7524. https://doi.org/10.1175/jcli-d-20-0948.1

Thilakarathne, M., & Sridhar, V. (2017). Characterization of future drought conditions in the Lower Mekong River Basin. *Weather and Climate Extremes*, *17*, 47–58. https://doi.org/10.1016/j.wace.2017.07.004

Touma, D., Ashfaq, M., Nayak, M. A., Kao, S. C., & Diffenbaugh, N. S. (2015). A multi-model and multi-index evaluation of drought characteristics in the 21st century. *Journal of Hydrology*, *526*, 196–207. https://doi.org/10.1016/j.jhydrol.2014.12.011

Ukkola, A. M., De Kauwe, M. G., Roderick, M. L., Abramowitz, G., & Pitman, A. J. (2020). Robust Future Changes in Meteorological Drought inCMIP6Projections Despite Uncertainty in Precipitation. *Geophysical Research Letters*, *47*(11). https://doi.org/10.1029/2020gl087820

Vicente-Serrano, S. M., Begueria, S., & Lopez-Moreno, J. I. (2010). A Multiscalar Drought Index Sensitive to Global Warming: The Standardized Precipitation Evapotranspiration Index. *Journal of Climate*, *23*(7), 1696–1718. https://doi.org/10.1175/2009jcli2909.1

Vicente-Serrano, S. M., Quiring, S. M., Pena-Gallardo, M., Yuan, S. S., & Dominguez-Castro, F. (2020). A review of environmental droughts: Increased risk under global warming? *Earth-Science Reviews*, *201*. https://doi.org/10.1016/j.earscirev.2019.102953

van Vuuren, D. P., Kriegler, E., O'Neill, B. C., Ebi, K. L., Riahi, K., Carter, T. R., et al. (2014). A new scenario framework for Climate Change Research: scenario matrix architecture. *Climatic Change*, *122*(3), 373–386. https://doi.org/10.1007/s10584-013-0906-1

Wang, T., Tu, X. J., Singh, V. P., Chen, X. H., & Lin, K. R. (2021). Global data assessment and analysis of drought characteristics based on CMIP6. *Journal of Hydrology*, *596*. https://doi.org/10.1016/j.jhydrol.2021.126091

WMO. (2021). *WMO Atlas of Mortality and Economic Losses from Weather, Climate and Water Extremes (1970–2019)*. Geneva, CH: World Meteorological Organization.

Yan, D. H., Wang, K., Qin, T. L., Weng, B. S., Wang, H., Bi, W. X., et al. (2019). A data set of global river networks and corresponding water resources zones divisions (Version 6) [Dataset]. Figshare. https://doi.org/10.6084/m9.figshare.8044184.v6

Yao, J. Q., Zhao, Y., Chen, Y. N., Yu, X. J., & Zhang, R. B. (2018). Multi-scale assessments of droughts: A case study in Xinjiang, China. *Science of the Total Environment*, *630*, 444–452. https://doi.org/10.1016/j.scitotenv.2018.02.200

Yin, Q., Wang, J. F., Ren, Z. P., Li, J., & Guo, Y. M. (2019). Mapping the increased minimum mortality temperatures in the context of global climate change. *Nature Communications*, *10*. https://doi.org/10.1038/s41467-019-12663-y

Yin, Y. Y., Gao, Y., Lin, D. G., Wang, L., Ma, W. D., & Wang, J. A. (2021). Mapping the Global-Scale Maize Drought Risk Under Climate Change Based on the GEPIC-Vulnerability-Risk Model. *International Journal of Disaster Risk Science*, *12*(3), 428–442. https://doi.org/10.1007/s13753-021-00349-3

Yue, T. X., Fan, Z. M., & Liu, J. Y. (2005). Changes of major terrestrial ecosystems in China since 1960. *Global and Planetary Change*, *48*(4), 287–302. https://doi.org/10.1016/j.gloplacha.2005.03.001

Yue, T. X., Fan, Z. M., Liu, J. Y., & Wei, B. X. (2006). Scenarios of major terrestrial ecosystems in China. *Ecological Modelling*, *199*(3), 363–376. https://doi.org/10.1016/j.ecolmodel.2006.05.026

Yue, T. X., Fan, Z. M., & Liu, J. Y. (2007). Scenarios of land cover in China. *Global and Planetary Change*, *55*(4), 317–342. https://doi.org/10.1016/j.gloplacha.2006.10.002

Zhang, Q., Yao, Y. B., Wang, Y., Wang, S. P., Wang, J. S., Yang, J. H., et al. (2019). Characteristics of drought in Southern China under climatic warming, the risk, and countermeasures for prevention and control. *Theoretical and Applied Climatology*, *136*(3–4), 1157–1173. https://doi.org/10.1007/s00704-018-2541-2

Zhang, X., Wei, C. H., Obringer, R., Li, D. R., Chen, N. C., & Niyogi, D. (2017). Gauging the Severity of the 2012 Midwestern US Drought for Agriculture. *Remote Sensing*, *9*(8). https://doi.org/10.3390/rs9080767

Zheng, H. X., Chiew, F. H. S., Charles, S., & Podger, G. (2018). Future climate and runoff projections across South Asia from CMIP5 global climate models and hydrological modelling. *Journal of Hydrology-Regional Studies*, *18*, 92–109. https://doi.org/10.1016/j.ejrh.2018.06.004

[Earth's Future]

Supporting Information for

Projecting global drought risk under various SSP-RCP scenarios

Zhiling Zhou[1], Liping Zhang[1,2]*, Jie Chen[1], Dunxian She[1,2], Gangsheng Wang[1,2], Qin Zhang[1], Jun Xia[1,2], Yanjun Zhang[1,2]

[1]State Key Laboratory of Water Resources and Hydropower Engineering Science, Wuhan University, Wuhan 430072, China.

[2]Institute for Water-Carbon Cycles and Carbon Neutrality, Wuhan University, Wuhan 430072, China.

Contents of this file

Figures S1 to S14

Introduction

The supporting information includes 14 supplementary figures to support our results and discussion (Figures S1-S14).

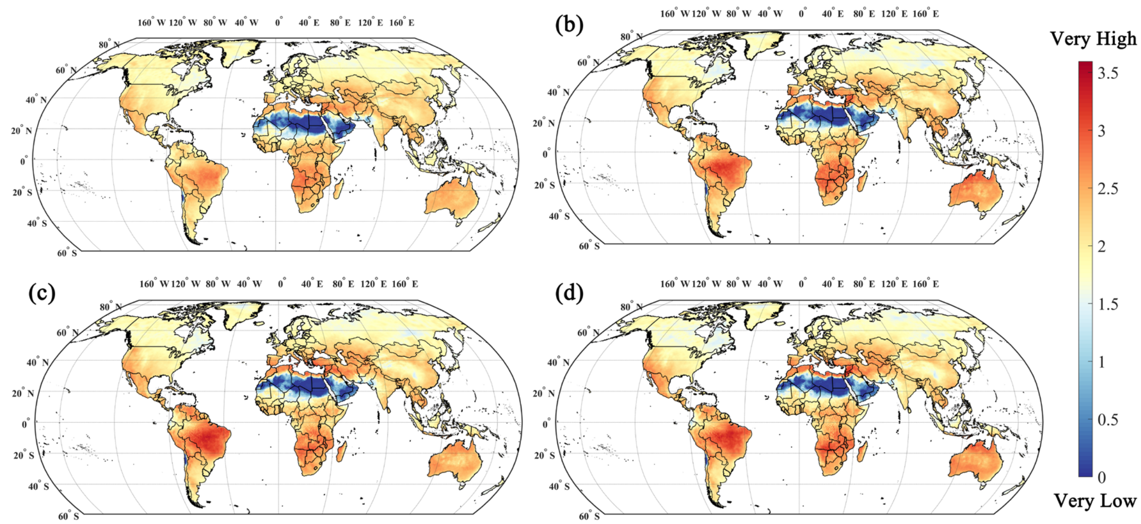

Figure S1. Distribution of the global drought hazard in (a) baseline period (1991–2014) and three projected periods: (b) 2021–2040, (c) 2041–2060, and (d) 2080–2100 under SSP1-2.6. SSP, shared socioeconomic pathway.

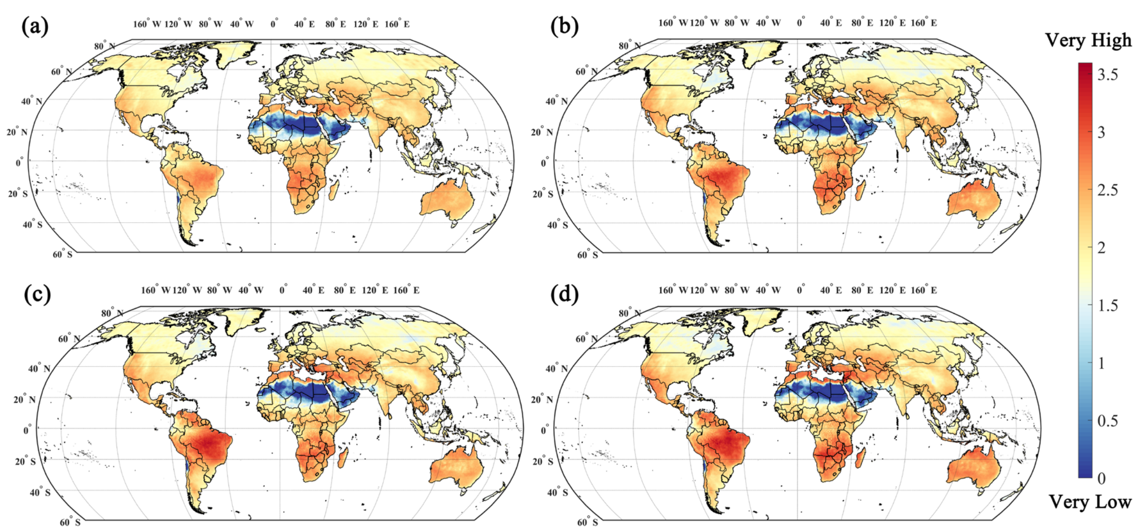

Figure S2. Distribution of the global drought hazard in (a) baseline period (1991–2014) and three projected periods: (b) 2021–2040, (c) 2041–2060, and (d) 2080–2100 under SSP3-7.0. SSP, shared socioeconomic pathway.

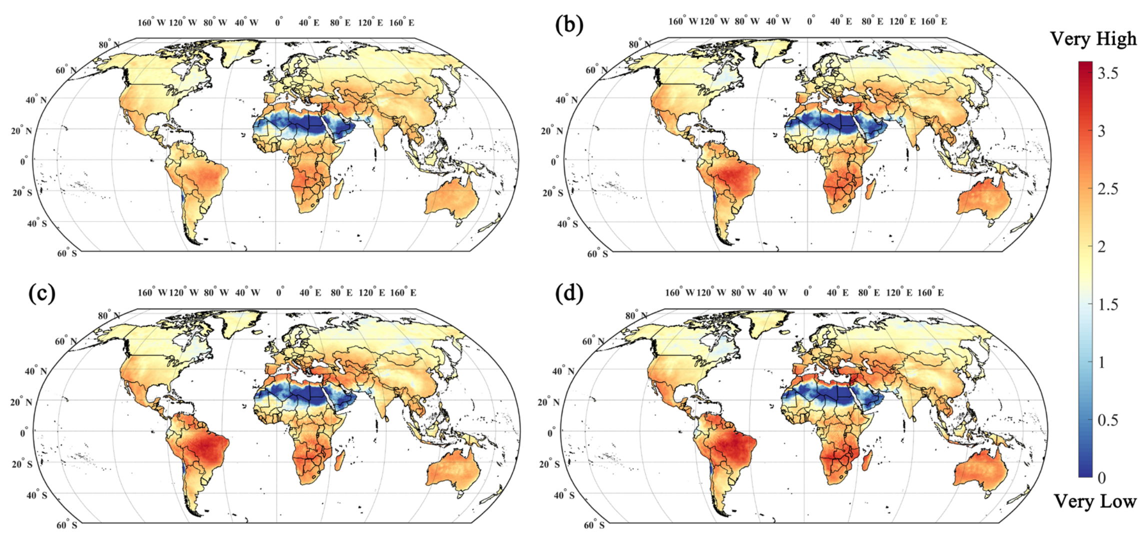

Figure S3. Distribution of the global drought hazard in (a) baseline period (1991–2014) and three projected periods: (b) 2021–2040, (c) 2041–2060, and (d) 2080–2100 under SSP5-8.5. SSP, shared socioeconomic pathway.

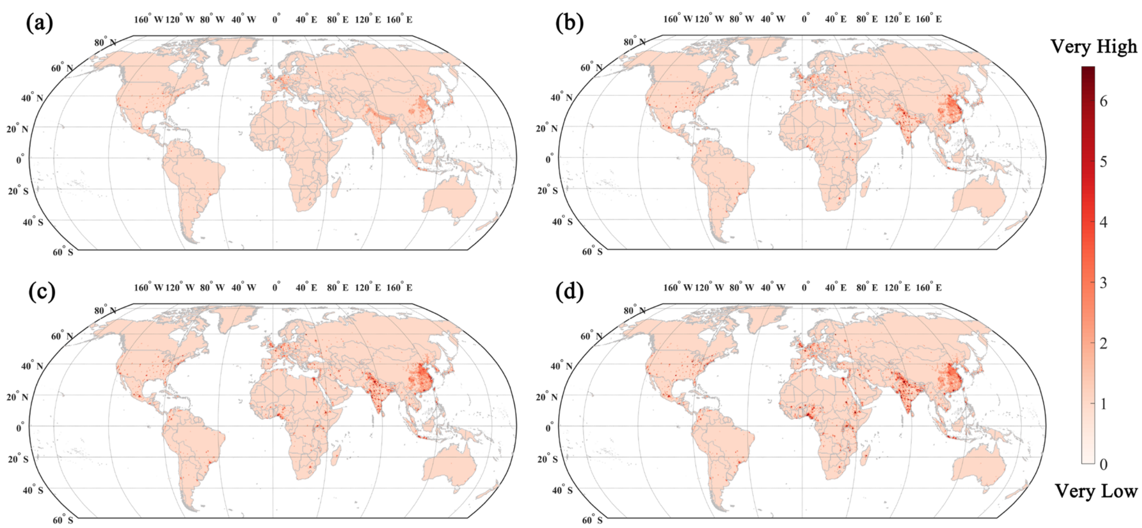

Figure S4. Distribution of the global drought exposure in (a) baseline period (1991–2014) and three projected periods: (b) 2021–2040, (c) 2041–2060, and (d) 2080–2100 under SSP1-2.6. SSP, shared socioeconomic pathway.

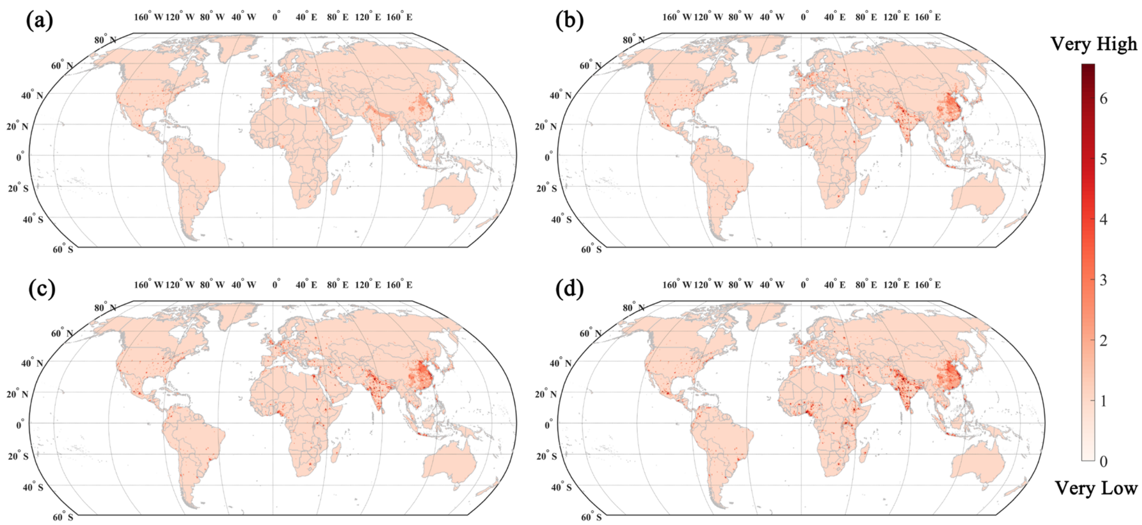

Figure S5. Distribution of the global drought exposure in (a) baseline period (1991–2014) and three projected periods: (b) 2021–2040, (c) 2041–2060, and (d) 2080–2100 under SSP3-7.0. SSP, shared socioeconomic pathway.

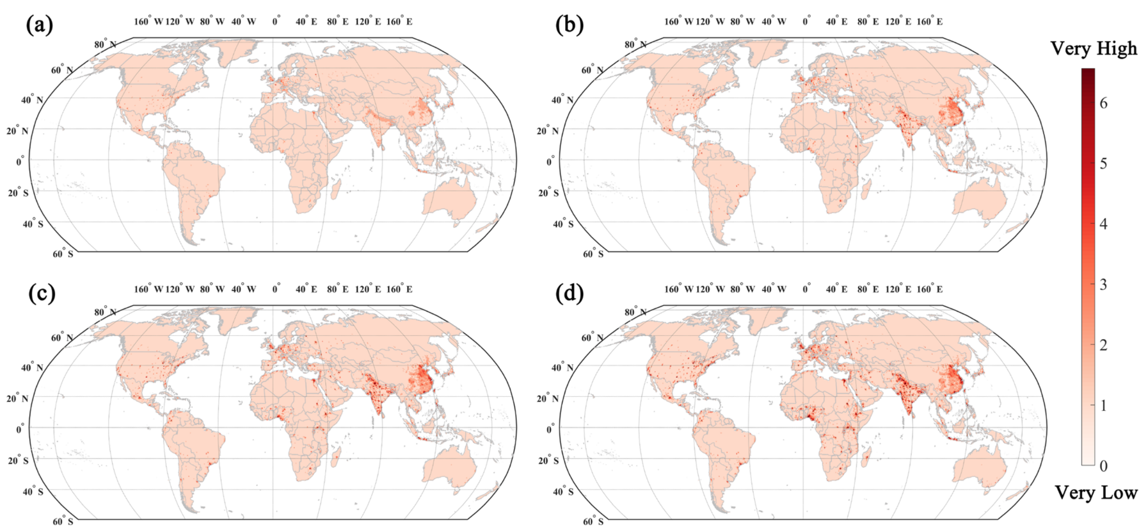

Figure S6. Distribution of the global drought exposure in (a) baseline period (1991–2014) and three projected periods: (b) 2021–2040, (c) 2041–2060, and (d) 2080–2100 under SSP5-8.5. SSP, shared socioeconomic pathway.

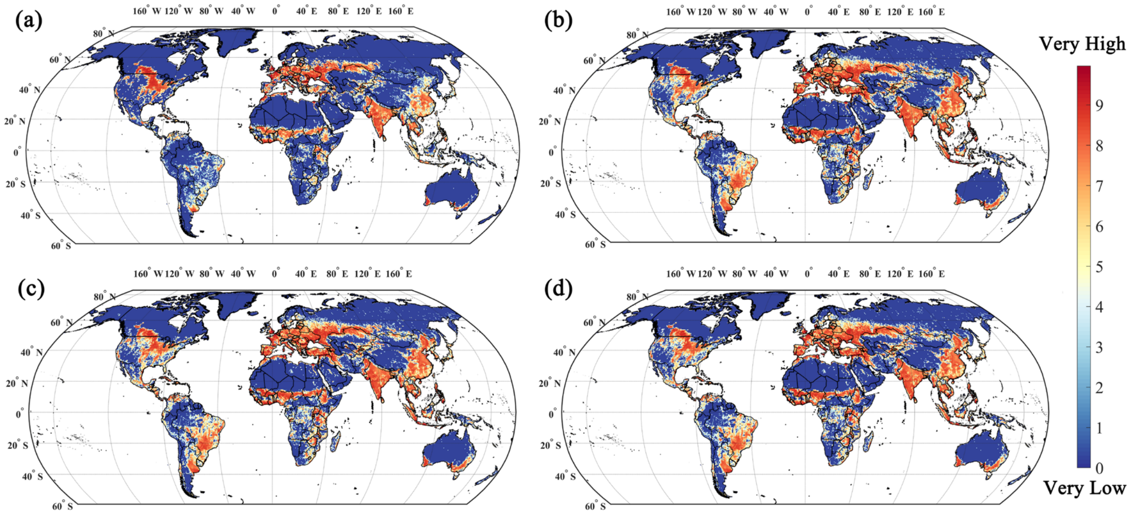

Figure S7. Distribution of the global drought vulnerability in (a) baseline period (1991–2014) and three projected periods: (b) 2021–2040, (c) 2041–2060, and (d) 2080–2100 under SSP1-2.6. SSP, shared socioeconomic pathway.

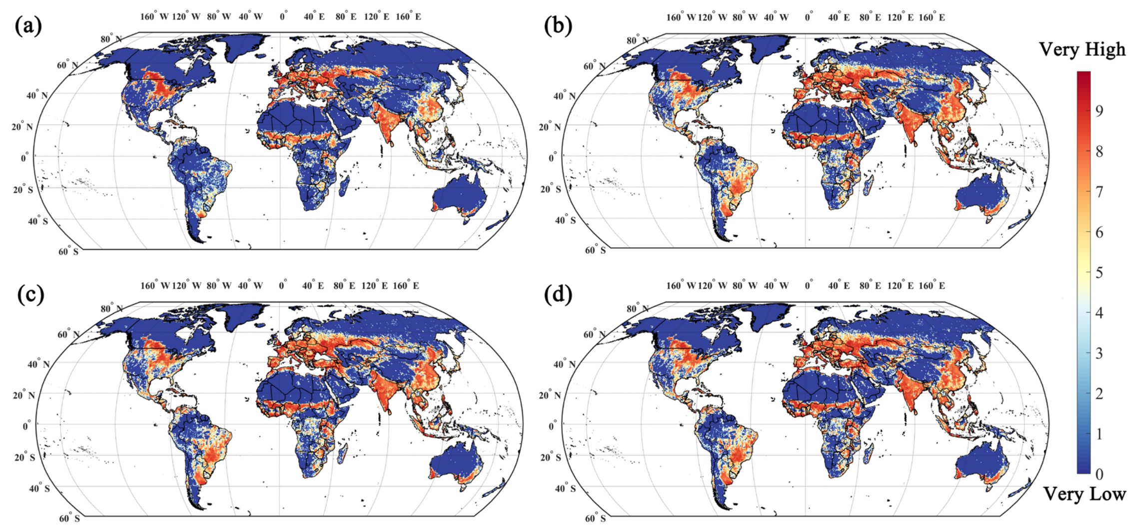

Figure S8. Distribution of the global drought vulnerability in (a) baseline period (1991–2014) and three projected periods: (b) 2021–2040, (c) 2041–2060, and (d) 2080–2100 under SSP3-7.0. SSP, shared socioeconomic pathway.

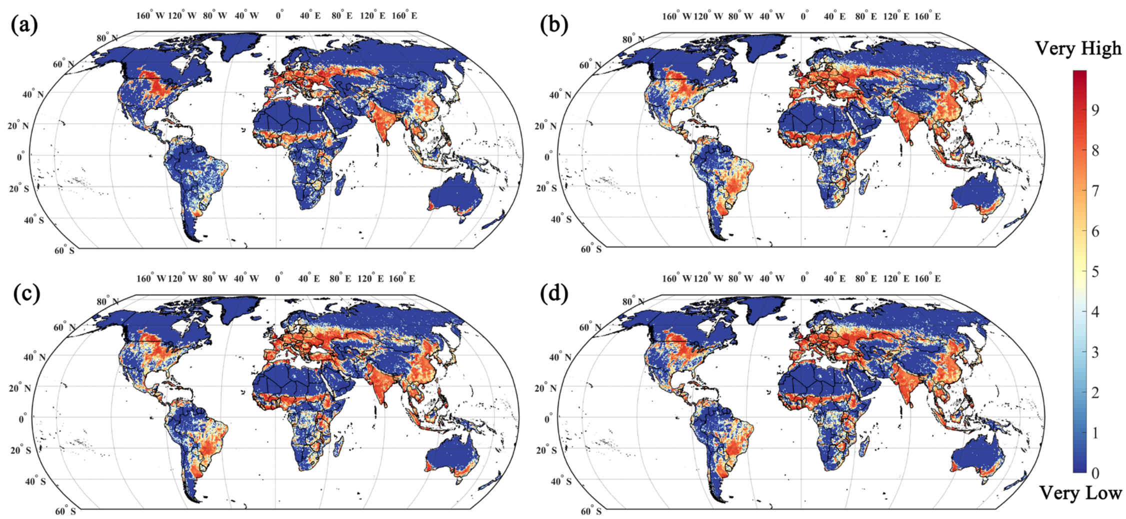

Figure S9. Distribution of the global drought vulnerability in (a) baseline period (1991–2014) and three projected periods: (b) 2021–2040, (c) 2041–2060, and (d) 2080–2100 under SSP5-8.5. SSP, shared socioeconomic pathway.

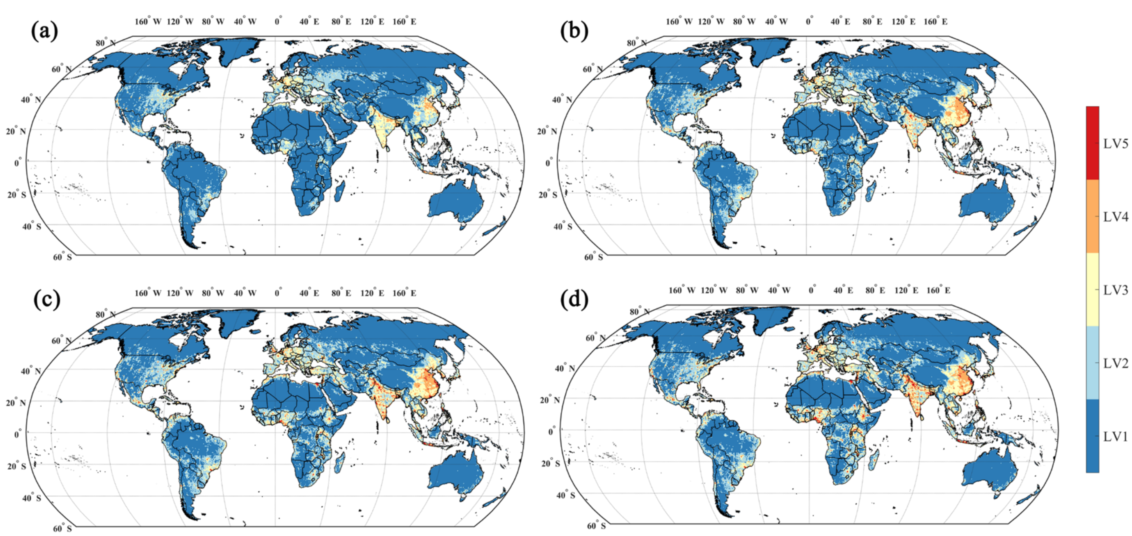

Figure S10. Distribution of the global drought risk in (a) baseline period (1991–2014) and three projected periods: (b) 2021–2040, (c) 2041–2060, and (d) 2080–2100 under SSP1-2.6. SSP, shared socioeconomic pathway; LV, level.

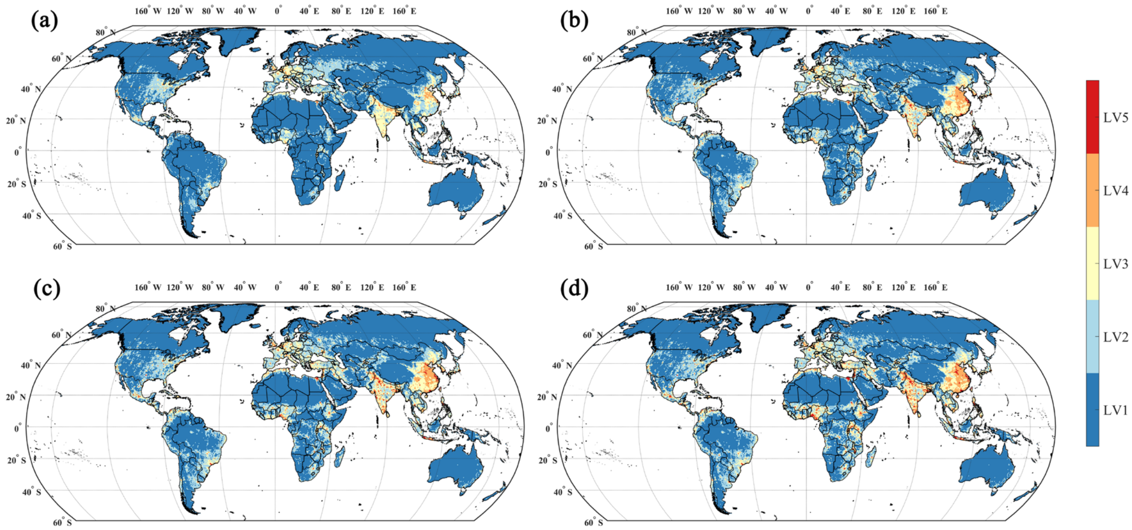

Figure S11. Distribution of the global drought risk in (a) baseline period (1991–2014) and three projected periods: (b) 2021–2040, (c) 2041–2060, and (d) 2080–2100 under SSP3-7.0. SSP, shared socioeconomic pathway; LV, level.

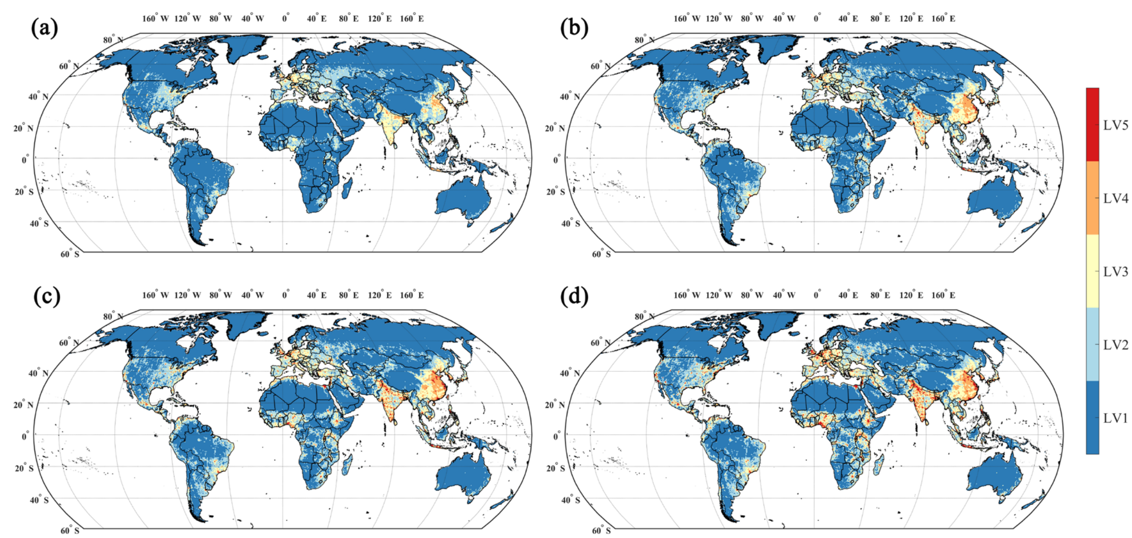

Figure S12. Distribution of the global drought risk in (a) baseline period (1991–2014) and three projected periods: (b) 2021–2040, (c) 2041–2060, and (d) 2080–2100 under SSP5-8.5. SSP, shared socioeconomic pathway; LV, level.

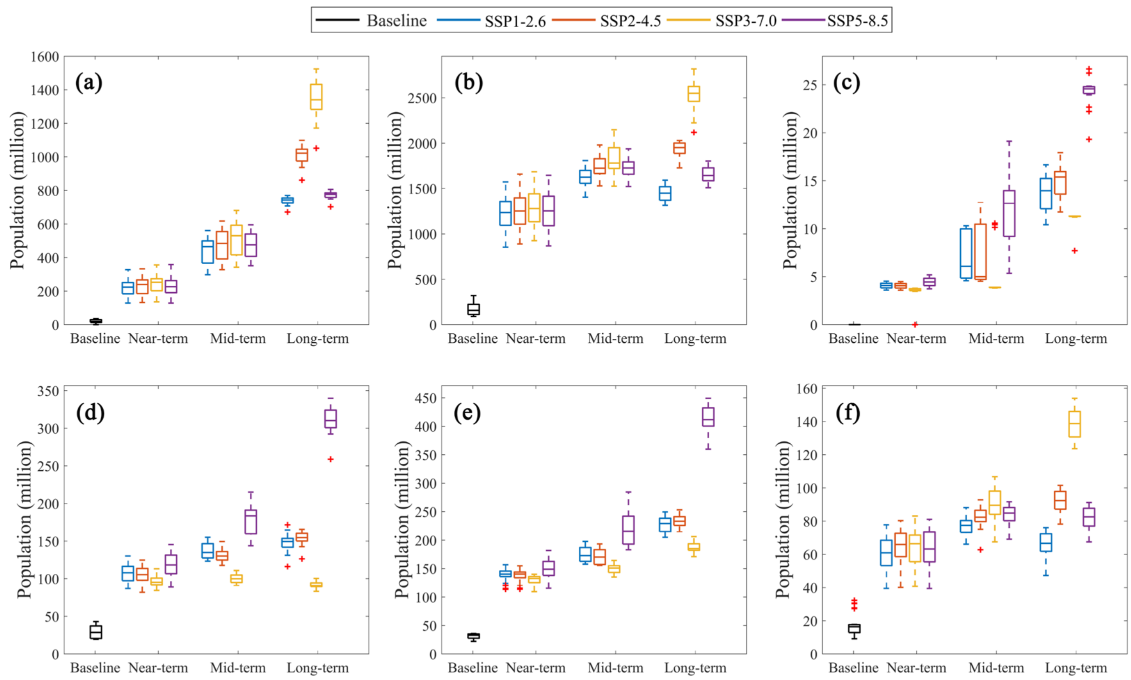

Figure S13. The total population under drought risk Level 5 for (a) Africa, (b) Asia, (c) Australia, (d) Europe, (e) North America, and (f) South America in the baseline period (1991-2014), near-term (2021–2040), mid-term (2041–2060), and long-term (2080–2100) under SSP1-2.6, SSP2-4.5, SSP3-7.0, and SSP5-8.5. SSP, shared socioeconomic pathway.

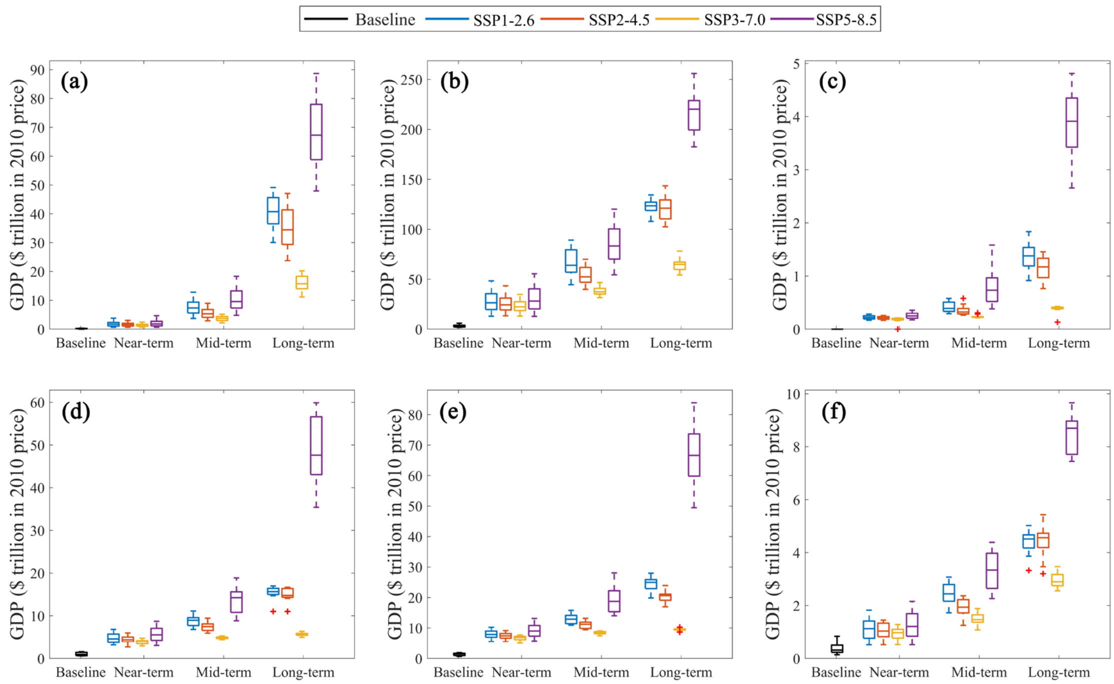

Figure S14. The total GDP under drought risk Level 5 for (a) Africa, (b) Asia, (c) Australia, (d) Europe, (e) North America, and (f) South America in the baseline period (1991-2014), near-term (2021–2040), mid-term (2041–2060), and long-term (2080–2100) under SSP1-2.6, SSP2-4.5, SSP3-7.0, and SSP5-8.5. GDP, Gross Domestic Product; SSP, shared socioeconomic pathway.